TABLE OF CONTENTS

I.	INTRODUCTION	1	1/A9
II.	MATHEMATICAL MODEL	4	1/A12
III.	SOIDUM CHLORIDE AND FORMATION OF ADVECTION FOG	8	1/B2
	A. Numbers of Nuclei as Variable	12	1/B6
	B. Mass of Nucleus as Variable	19	1/B13
	C. Radius of Nucleus as Variable	26	1/C6
IV.	AEROSOL PARTICLES WITH HIGHER RATIO OF THE VAN'T HOFF FACTOR TO MOLECULAR WEIGHT THAN SODIUM CHLORIDE AND THE FORMATION OF ADVECTION FOG	26	1/C6
	A. Case with Concentration of 50 $\mu g/m^3$ and Size of Nuclei of 0.5 μm Radius	33	1/C13
	B. Case with Concentration of 100 $\mu g/m^3$ and Size of Nuclei of 1 μm Radius	37	1/D5
V.	AEROSOL PARTICLES WITH LOWER RATIO OF VAN'T HOFF FACTOR TO MOLECULAR WEIGHT THAN SODIUM CHLORIDE AND THE FORMATION OF ADVECTION FOG	37	1/D5
	A. Case with Concentration of 100 $\mu g/m^3$ and Size of Nuclei of 0.5 μm Radius	44	1/D2
	B. Case with Concentration of 100 $\mu g/m^3$ and the Size of the Nuclei of 1 μm Radius	51	1/E5
Vi.	CONCLUSIONS AND DISCUSSIONS	51	1/E5
	REFERENCES	57	1/E11

Stim 239-H-14
NAS 1.26:3085
JAN 23 1979
COMPLETED
ORIGINAL

NASA Contractor Report 3085

Microfilmed From
Best Available Copy

Hygroscopic Chemicals and the Formation of Advection Warm Fog - A Numerical Simulation

R. J. Hung and G. S. Liaw

CONTRACT NAS8-31729
DECEMBER 1978

NASA

NASA Contractor Report 3085

Microfilmed From
Best Available Copy

Hygroscopic Chemicals and the Formation of Advection Warm Fog - A Numerical Simulation

R. J. Hung and G. S. Liaw
The University of Alabama in Huntsville
Huntsville, Alabama

Prepared for
George C. Marshall Space Flight Center
under Contract NAS8-31729

National Aeronautics
and Space Administration

Scientific and Technical
Information Office

1978

ACKNOWLEDGMENT

The authors express their gratitude to Mr. O. H. Vaughan, Jr., and Mr. Dennis W. Camp of the Atmospheric Science Division, NASA/Marshall Space Flight Center. They are also indebted to Mr. John H. Enders of the Aviation Safety Technology Branch, Office of Advanced Research and Technology (OAST), NASA Headquarters, for his support of this research. The research reported herein was supported under Contract NAS8-31729.

LIST OF FIGURES

Figure No.		Page
1	Horizontal wind velocity profile for condensation nuclei, NaCl, with mass of nucleus 10^{-6} µg, radius of nucleus 0.5 µm, and number density 50 particles/cm^3, at time t = 1 hr.	10
2	Horizontal wind velocity profile for condensation nuclei, NaCl, with mass of nucleus 10^{-6} µg, radius of nucleus 0.5 µm, and number density 50 particles/cm^3, at time t = 2 hrs.	11
3	Comparison of temperature profiles of condensation nuclei, NaCl, between numbers of nuclei, 50 and 100 particles/cm^3, with constant mass of nucleus 10^{-6} µg, and radius of nucleus 0.5 µm, at time t = 1 hr.	13
4	Comparison of temperature profiles of condensation nuclei, NaCl, between numbers of nuclei, 50 and 100 particles/cm^3, with constant mass of nucleus 10^{-6} µg, and radius of nucleus 0.5 µm, at time t = 2 hrs.	14
5	Visibility profile due to condensation nuclei, NaCl, with mass of nucleus 10^{-6} µg, radius of nucleus 0.5 µm, and number density 50 particles/cm^3, at time t = 1 hr.	15
6	Visibility profile due to condensation nuclei, NaCl, with mass of nucleus 10^{-6} µg, radius of nucleus 0.5 µm, and number density 50 particles/cm^3, at time t = 2 hrs.	16
7	Visibility profile due to condensation nuclei, NaCl, with mass of nucleus 10^{-6} µg, radius of nucleus 0.5 µm, and number density 100 particles/cm^3, at time t = 1 hr.	17
8	Visibility profile due to condensation nuclei, NaCl, with mass of nucleus 10^{-6} µg, radius of nucleus 0.5 µm, and number density 100 particles/cm^3, at time t = 2 hrs.	18
9	Comparison of temperature profiles of condensation nuclei, NaCl, between masses of nuclei, 10^{-6} and 10^{-7} µg, with constant radius of nucleus 1 µm, and number density 100 particles/cm^3, at time t = 1 hr.	20
10	Comparison of temperature profiles of condensation nuclei, NaCl, between masses of nuclei, 10^{-6} and 10^{-7} µg, with constant radius of nucleus 1 µm, and number density 100 pa-ticles/cm^3, at time t = 2 hrs.	21
11	Visibility profile due to condensation nuclei, NaCl, with mass of nucleus 10^{-6} µg, radius of nucleus 1 µm, and number density 100 particles/cm^3, at time t = 1 hr.	22

Figure No.		Page
12	Visibility profile due to condensation nuclei, NaCl, with mass of nucleus 10^{-6} µg, radius of nucleus 1 µm, and number density 100 particles/cm^3, at time t = 2 hrs.	23
13	Visibility profile due to condensation nuclei, NaCl, with mass of nucleus 10^{-7} µg, radius of nucleus 1 µm, and number density 100 particles/cm^3, at time t = 1 hr.	24
14	Visibility profile due to condensation nuclei, NaCl, with mass of nucleus 10^{-7} µg, radius of nucleus 1 µm, and number density 100 particles/cm^3, at time t = 2 hrs.	25
15	Comparison of temperature profiles of condensation nuclei, NaCl, between radii of nuclei, 1 and 0.5 µm, with corresponding masses of nuclei, 4.45×10^{-6} and 5.56×10^{-7} µg, respectively, and with constant number density 100 particles/cm^3, at time t = 1 hr.	27
16	Comparison of temperature profiles of condensation nuclei, NaCl, between radii of nuclei, 1 and 0.5 µm, with corresponding masses of nuclei, 4.45×10^{-6} and 5.56×10^{-7} µg, respectively, and with constant number density 100 particles/cm^3, at time t = 2 hrs.	28
17	Visibility profile due to condensation of nuclei, NaCl, with mass of nucleus 5.56×10^{-7} µg, radius of nucleus 0.5 µm, and number density 100 particles/cm^3, at time t = 1 hr.	29
18	Visibility profile due to condensation nuclei, NaCl, with mass of nucleus 5.56×10^{-7} µg, radius of nucleus 0.5 µm, and number density 100 particles/cm^3, at time t = 2 hrs.	30
19	Visibility profile due to condensation nuclei, NaCl, with mass of nucleus 4.45×10^{-6} µg, radius of nucleus 1 µm, and number density 100 particles/cm^3, at time t = 1 hr.	31
20	Visibility profile due to condensation nuclei, NaCl, with mass of nucleus 4.45×10^{-6} µg, radius of nucleus 1 µm, and number density 100 particles/cm^3, at time t = 2 hrs.	32
21	Comparison of temperature profiles between condensation nuclei, LiCl and NaCl, with the same mass of nucleus 10^{-6} µg, radius of nucleus 0.5 µm, and number density 50 particles/cm^3, at time t = 1 hr.	35
22	Comparison of temperature profiles between condensation nuclei, LiCl and NaCl, with the same mass of nucleus 10^{-6} µg, radius of nucleus 0.5 µm, and number density 50 particles/cm^3, at time t = 2 hrs.	36

Figure No.		Page
23	Visibility profile due to condensation nuclei, LiCl, with mass of nucleus 10^{-6} µg, radius of nucleus 0.5 µm, and number density 50 particles/cm^3, at time t = 1 hr.	38
24	Visibility profile due to condensation nuclei, LiCl, with mass of nucleus 10^{-6} µg, radius of nucleus 0.5 µm, and number density 50 particles/cm^3, at time t = 2 hrs.	39
25	Comparison of temperature profiles between conyensation nuclei, LiCl and NaCl, with the same mass of nucleus 10^{-6} µg, radius of nucleus 1 µm, and number density 100 particles/cm^3, at time t = 1 hr.	40
26	Comparison of temperature profiles between condensation nuclei, LiCl and NaCl, with the same mass of nucleus 10^{-6} µg, radius of nucleus 1 µm, and number density 100 particles/cm^3, at time t = 2 hrs.	41
27	Visibility profile due to condensation nuclei, LiCl, with mass of nucleus 10^{-6} µg, radius of nucleus 1 µm, and number density 100 particles/cm^3, at time t = 1 hr.	42
28	Visibility profile due to condensation nuclei, LiCl, with mass of nucleus 10^{-6} µg, radius of nucleus 1 µm, and number density 100 particles/cm^3, at time t = 2 hrs.	43
29	Comparison of temperature profiles between condensation nuclei, $Ca(NO_3)_2$ and NaCl, with the same mass of nucleus 10^{-6} µg, radius of nucleus 0.5 µm, and number density 100 particles/cm^3, at time t = 1 hr.	45
30	Comparison of temperature profiles between condensation nuclei, $Ca(NO_3)_2$ and NaCl, with the same mass of nucleus 10^{-6} µg, radius of nucleus 0.5 µm, and number density 100 particles/cm^3, at time t = 2 hrs.	46
31	Visibility profile due to condensation nuclei, $Ca(NO_3)_2$, with mass of nucleus 10^{-6} µg, radius of nucleus 0.5 µm, and number density 100 particles/cm^3, at time t = 1 hr.	47
32	Visibility profile due to condensation nuclei, $Ca(NO_3)_2$, with mass of nucleus 10^{-6} µg, radius of nucleus 0.5 µm, and number density 100 particles/cm^3, at time t = 2 hrs.	48
33	Visibility profile due to condensation nuclei, $CaCl_2$, with mass of nucleus 10^{-6} µg, radius of nucleus 0.5 µm, and number density 100 particles/cm^3, at time t = 1 hr.	49

Figure No.		Page
34	Visibility profile due to condensation nuclei, $CaCl_2$, with mass of nucleus 10^{-6} µg, radius of nucleus 0.5 µm, and number density 100 particles/cm^3, at time t = 2 hrs.	50
35	Comparison of temperature profiles between condensation nuclei, $CaCl_2$ and NaCl, with the same mass of nucleus 10^{-6} µg, radius of nucleus 1 µm, and number density 100 particles/cm^3, at time t = 1 hr.	52
36	Comparison of temperature profiles between condensation nuclei, $CaCl_2$ and NaCl, with the same mass of nucleus 10^{-6} µg, radius of nucleus 1 µm, and number density 100 particles/cm^3, at time t = 2 hrs.	53
37	Visibility profile due to condensation nuclei, $CaCl_2$, with mass of nucleus 10^{-6} µg, radius of nucleus 1 µm, and number density 100 particles/cm^3 at time t = 1 hr.	54
38	Visibility profile due to condensation nuclei, $CaCl_2$, with mass of nucleus 10^{-6} µg, radius of nucleus 1 µm, and number density 100 particles/cm at time t = 2 hrs.	55

LIST OF TABLE

Table No.		Page
1	Comparison of Ratio of Van't Hoff Factor to Molecular Weight for Some Typical Hygroscopic Materials	34

1. - INTRODUCTION

In the absence of aerosol particles and ions in the atmosphere, condensation of water vapor will occur only if the supersaturation reaches several hundred percent. However, in the atmosphere, there are abundant foreign particles to serve as ready-prepared nuclei for condensation and prevent the large supersaturations from being achieved. The peak supersaturation that will be attained in an air mass containing a population of condensation nuclei will depend upon the temperature and the rate of cooling of the air, and upon the concentration, size distribution, and nature of the particles (Mason, 1971).

Recently, the characteristics of aerosol particles have been extensively studied, and it is clear that atmospheric aerosols cover a wide range of particle sizes, from about 10^{-3} μm radius for the small ions consisting of a few neutral air molecules clustered around a charged molecule to more than 10 μm for the largest salt and dust particles. Their concentration also covers an enormous range, from less than 1000 per cm^3 over the ocean, to perhaps 10^6 per cm^3 in the highly polluted air of large industrial cities. The small ubiquitous ions almost certainly play no part in atmospheric condensation because of the very high supersaturation (about 300 percent) required for their activation, while particles of radius greater than 10 μm, having fall speeds of several cm/sec, are able to remain airborne for only a limited time (Mason, 1971).

The purpose of the present study was to numerically simulate how the concentration, particle size, mass of nuclei, and chemical composition would affect the dynamics of warm fog formation, in particular the formation of advection fog.

Among all fog occurrences worldwide, warm fog (temperature above the freezing point of water) accounts for about 95% (Sax, et al., 1975). Among the categories of fog according to the standpoint of dispersal, warm fog is the most stable cloud system in the atmosphere. In contrast to supercooled fog, there is no latent phase instability in warm fog that can be exploited to promote the artificial dissipation process. Warm fog dispersal methods are necessarily "brute force" in character. Whatever energy is required to dissipate the fog must be supplied by the dispersal method.

It is most economical to use computer simulation techniques to study the characteristics of warm fog, in particular how the microstructure of advection fog is influenced by the supersaturation spectrum of cloud condensation nuclei (CCN) in the air. Recently, Baker (1977) and Eadie et al. (1975) proposed boundary layer models of advection fog. In these models, water vapor in excess of the saturation amount is immediately and completely condensed (i.e., the air never becomes supersaturated) on a population of existing droplets.

Contrary to the boundary layer models treated by previous investigators, a one-dimensional Lagrangian model of the formation and evolution of droplet spectra in advection fog was proposed by Fitzgerald (1978). This model incorporates the physical processes governing the formation and evolution of fog droplets from a population of cloud condensation nuclei contained in a parcel which is advected with the wind. The effects of vertical diffusion transfer, momentum transfer, and energy transfer are completely ignored in this model.

In the present study, computer modeling of warm fog is used to investigate a two-dimensional model of fog formation and the evolution of droplet spectra. A description of the vertical and horizontal turbulent transfer of heat, moisture and momentum, together with the growth of fog droplets from a microphysical point of view, have been included in this model. Both advection and infrared radiation effects are also taken into account. The driving force for the fog formation is a prescribed time rate of cooling on the ground.

This model is being used to study how chemical composition, mass of nuclei, particle size, and the concentration of aerosol particles affect the formation and development of advection fog. The present model also can be used for prediction purposes using as input the following initial data: (1) temperature profile; (2) wind profile; (3) relative humidity; (4) cooling rate of the ground; (5) chemical composition, mass of nuclei, particle size and the concentration of CCN.

Numerical simulation of the formation of advection fog was accomplished using different input parameters such as the mass of the nuclei, particle size, number density and chemical composition.

The correlation of fog formation and CCN with different chemical compositions was investigated and compared with the results obtained from using sodium chloride nuclei. It was found that the value of the ratio of the Van't Hoff factor to molecular weight plays a very important role in the fog formation during nucleation and condensation time period. The formation of characteristics of advection fog using hygroscopic chemicals with various values of the ratio of the Van't Hoff factor to molecular weight were simulated and are discussed.

II. - MATHEMATICAL MODEL

A theoretical model has been developed which describes the evolution of potential temperature, water vapor content, liquid water content, and horizontal and vertical winds as determined by the processes of vertical turbulent transfer and horizontal advection of momentum, energy and moisture, as well as radiation cooling, growth of water droplets based on microphysical processes, and drop sedimentation.

The mathematical model is two-dimensional in the X-Z plane, and the boundary layer model is assumed. All the quantities are uniform in the Y direction. The diffusivity coefficient is the same for liquid water droplets as for vapor.

The fundamental equations governing the macrophysical processes of the evolution of wind components, water vapor content, liquid water content and potential temperature under the influences of vertical turbulent diffusion transfer, turbulent momentum transfer and turbulent energy transfer can be expressed in the following three sets of conservation equations:

(a) Mass conservation equation of the air and diffusion equations for water vapor and liquid water contents

$$\frac{\partial U_x}{\partial x} + \frac{\partial U_z}{\partial z} = 0 \qquad (1)$$

$$\frac{\partial C_{va}}{\partial t} = - U_x \frac{\partial C_{va}}{\partial x} - U_z \frac{\partial C_{va}}{\partial z} + \frac{\partial}{\partial z} \left(K_d \frac{\partial C_{va}}{\partial z} \right) - F_{cv} \qquad (2)$$

$$\frac{\partial C_{wa}}{\partial t} = - U_x \frac{\partial C_{wa}}{\partial x} - U_z \frac{\partial C_{wa}}{\partial z} + \frac{\partial}{\partial z} \left(K_d \frac{\partial C_{wa}}{\partial z} \right)$$

$$+ \frac{\partial}{\partial z} (U_t C_{wa}) + F_{cw}$$

(b) Momentum conservation equations

$$\frac{\partial U_x}{\partial t} = - U_x \frac{\partial U_x}{\partial x} - U_z \frac{\partial U_x}{\partial z} - \frac{1}{\rho} \frac{\partial p}{\partial x} + \frac{\partial}{\partial z} \left(K_m \frac{\partial U_x}{\partial z} \right) + f U_y \quad (4)$$

$$\frac{\partial U_y}{\partial t} = - U_x \frac{\partial U_y}{\partial x} - U_z \frac{\partial U_y}{\partial z} + \frac{\partial}{\partial z} \left(K_m \frac{\partial U_y}{\partial z} \right) + f(U_g - U_x) \quad (5)$$

$$\frac{\partial U_z}{\partial t} = - U_x \frac{\partial U_z}{\partial x} - U_z \frac{\partial U_z}{\partial z} - \frac{1}{\rho} \frac{\partial P}{\partial z} + \frac{\partial}{\partial z} \left(K_m \frac{\partial U_z}{\partial z} \right) \quad (6)$$

(c) Energy conservation equation

$$\frac{\partial \theta}{\partial t} = - U_x \frac{\partial \theta}{\partial x} - U_z \frac{\partial \theta}{\partial z} + \frac{\partial}{\partial z} \left(K_h \frac{\partial \theta}{\partial z} \right)$$

$$+ \frac{1}{\rho C_p} \left(\frac{1000}{P} \right)^{2/7} \left(L F_{cv} \rho - \frac{\partial R_f}{\partial z} \right) \quad (7)$$

where

$$C_{va} = \frac{\rho_v}{\rho} \quad (8)$$

$$C_{wa} = \frac{\rho_w}{\rho} 4\pi \left[\int_0^\infty N(r) r^2 dr - \frac{1}{3} \sum_i N_i r_{o_i}^3 \right] . \quad (9)$$

Here, U_x is the wind component in the horizontal x-direction; U_y, the wind component in the horizontal y-direction; U_z, the wind component in the vertical z-direction; C_{va}, water vapor-air mixing ratio; C_{wa}, liquid water-air mixing ratio; K_m, turbulent exchange coefficient for vertical turbulent transfer of momentum; K_d, turbulent exchange coefficient for turbulent

transfer of water vapor diffusion and liquid water diffusion; K_h, turbulent exchange coefficient for turbulent transfer of heat flux; f, Coriolis parameter; U_g, velocity of geostropic wind; F_{cv}, source function for condensation and evaporation for water vapor; F_{cw}, source function for condensation and evaporation for liquid water; U_t, mean terminal velocity of fog drops; ρ_v, water vapor density; ρ_w, liquid water density; N, number density of water droplet which is a function of droplet size; r, radius of water droplet; r_o, radius of nucleus; θ, the potential temperature; and R_f, net upward flux of infrared radiation.

Equation (1) is the expression of incompressible fluid for the continuity equation of dry air. This expression is true only when the wind velocity is much less than the speed of sound. In this case, the wind velocity up to 100 m altitude is in general less than 10m/sec which is less than 3% of the speed of sound.

The change of the water droplet radius, in Equation (9), due to condensation/evaporation is governed by microphysical processes, and is given by (Fletcher, 1966)

$$r \frac{dr}{dt} = G \left(SS - \frac{a}{r} + \frac{b}{r^3}\right) \tag{10}$$

where

$$G = K_d \frac{\rho_v}{\rho_w} \left[1 + \frac{K_d L^2 \rho_v M_o}{R_v T^2 k}\right] \tag{11}$$

Here

$$a = \frac{2\sigma M_o}{\rho_w R_v T} \approx 3.3 \times 10^{-5} \frac{1}{T} \tag{12}$$

$$b = \frac{i m M_o}{\frac{4}{3}\pi \rho_w M} \simeq 4.3\, i \frac{m}{M} \tag{13}$$

$$SS = S - 1 \tag{14}$$

and

$$S = \frac{P_v}{P_v^{sat}} = \frac{\rho_v}{\rho_v^{sat}} = C_{va} \frac{\rho}{\rho_v^{sat}} \tag{15}$$

at corresponding temperature. Here, a denotes the effect of water droplet curvature which is a function of temperature; b, hygroscopic material solution on the growth of the water droplet; k, the thermal conductivity of air; R_v the gas constant for water vapor; σ, surface tension of the water droplet; M_o, gram molecular weight of water; m, the mass of hygroscopic nucleus; i, Van't Hoff factor of hygroscopic nucleus; M, gram molecular weight of the hygroscopic nucleus; SS, the supersaturation ratio; S, the saturation ratio; ρ_v^{sat}, saturation water vapor density at temperature T. The approximate expressions given in Equations (10)-(15) are accepted simplifications of the more complicated relationships that are thoroughly described by Fletcher (1966) (Weinstein and Silverman, 1973).

The fundamental equations governing the macrophysical processes given in Equations (1)-(7) are similar to the fundamental equations employed by Eadie, et al., (1975) with three exceptions which were not considered by them. These three exceptions are as follows: (1) the mass conservation equation of air; (2) the vertical wind component (This difference makes the convective term become $U_x(\partial/\partial x) + U_z(\partial/\partial z)$ instead of $U_x(\partial/\partial x)$, as for their case. Reinstallation of $U_z(\partial/\partial z)$ is particularly

important because of the strong vertical dependence in our case. This will ensure the effect of vertical convection due to steep vertical gradients.); (3) The evolution of water vapor-air mixture and liquid water-air mixture which is governed by the dynamics of turbulent thermal diffusion, K_d, rather than the turbulent heat flux exchange, K_h, which they used.

The application of the macroscopic equations (1)-(7), in particular the evolution of the turbulent transport coefficients, for the study of the dynamical behaviors of warm fog are given in Hung and Vaughan (1977). The microscopic equations (10)-(15), in particular the initial stage of the growth of the water droplets, is discussed in Hung and Huckle (1977); while the growth and decay of water droplets in terms of the seeding of hygroscopic chemicals and aerosol particles is discussed in Hung et al. (1978).

III. - SODIUM CHLORIDE AND FORMATION OF ADVECTION FOG

It was discussed by Japanese workers that the prominent nuclei of fog which occurs in coastal areas is sodium chloride with masses between 10^{-7} and 10^{-6} μg (Isono, 1957; also Mason, 1971). Sodium chloride has also been proposed as one of the most important seeding materials for fog modification. In this study, sodium chloride with various spectra was used to numerically simulate the formation of advection fog.

In this computation, the method of implicit integration of the finite difference equations has been used to solve the governing partial differential equations. The numerical technique is essentially similar to that of Richtmyer (1957). The initial values of the wind profile,

temperature profile, and relative humidity use the results of field measurements taken along the California coast by Mack et al. (1973), Mack et al. (1974), and Mack et al. (1975).

In the horizontal geometrical x-coordinate, the initial temperature at the ground was 14°C everywhere, and decreased to 13°C within 2 hours linearly at the location of the temperature sink 3 km $\leq x \leq$ 6 km. The source terms of Equations (2) and (3) were assumed to be zero at time, t = 0; and $F_{cv} = F_{cw}$ at time, t > 0. Reasonably large time steps have been used to obtain a computationally stable solution.

The visibility is computed by using the relation

$$\text{visibility} = \frac{3.912}{\beta} \quad \text{(m)} \tag{16}$$

where β is related to the drop size distribution, N(r), and Mie scattering efficiency, S_M, which is important for droplets larger than 1 μm, according to

$$\beta = 4\pi \int_0^\infty S_M N(r)\, r dr. \tag{17}$$

A wide spectra of sodium chloride, in which concentrations in the range of 10 to 100 particles/cm^3; masses of nuclei in the range of 10^{-4} to 10^{-9} μg; and radius of nuclei in the range of 0.1 to 5 μm, were chosen for the computation.

It is quite interesting to show how the wind profile varies as the nucleation and condensation proceed. Figures 1 and 2 illustrate horizontal velocity profiles for times, t = 1 hr, and t = 2 hrs, respectively.

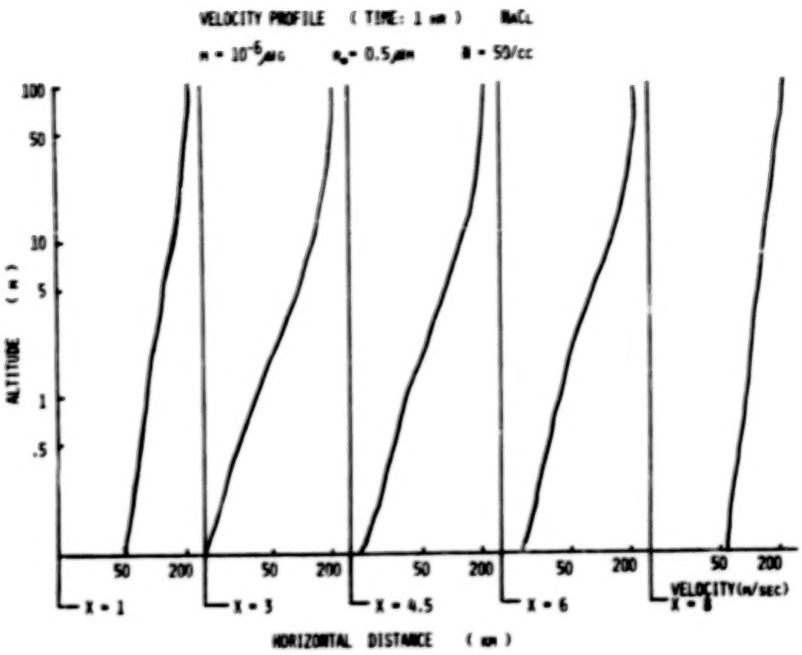

Figure 1. Horizontal wind velocity profile for condensation nuclei, NaCl, with mass of nucleus 10^{-6} μg, radius of nucleus 0.5 μm, and number density 50 particles/cm^3, at time t = 1 hr.

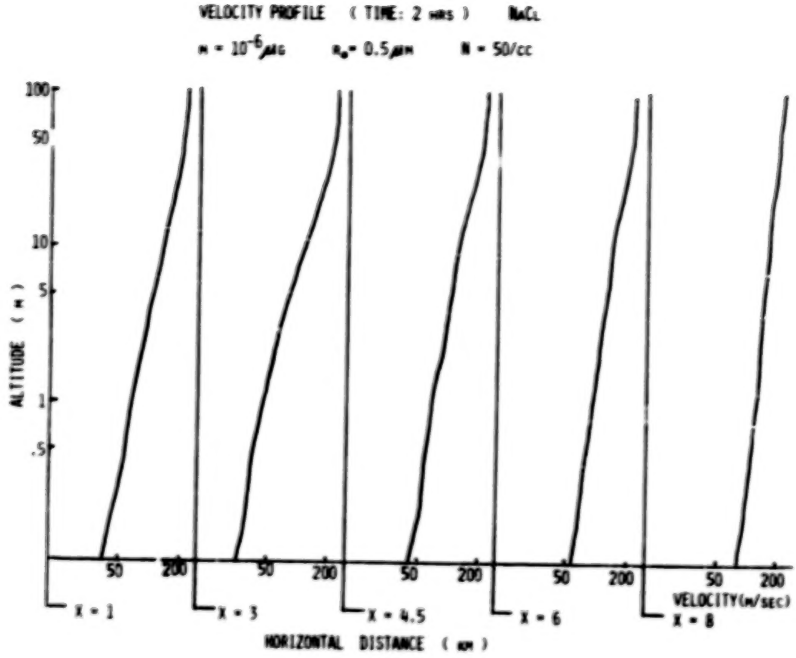

Figure 2. Horizontal wind velocity profile for condensation nuclei, NaCl, with mass of nucleus 10^{-6} μg, radius of nucleus 0.5 μm, and number density 50 particles/cm^3, at time t = 2 hrs.

This computation is based on the spectrum of sodium chloride with a number of nuclei, 50 particles/cm^3; mass of nucleus, 10^{-6} μg; and radius of nucleus, 0.5 μm. These figures show that the cooling effect at the ground acts as a major force to drive the nucleation and condensation processes through a strong exchange in vertical diffusion, vertical turbulent momentum, and vertical turbulent energy transport. These enhanced vertical transports cause highly disturbed wind profiles downstream and inside the boundary layer portion of the temperature sink.

Two-dimensional expressions of temperature profile and visibility are shown, assuming one out of three parameters (numbers of nuclei, mass of nucleus, and radius of nucleus) as a variable.

A. Numbers of Nuclei as Variable

Sodium chloride with nucleus mass, 10^{-6} μg, and size, 0.5 μm radius, is chosen as the example. Figures 3 and 4 compare the temperature profiles for number densities of 50 and 100 particles/cm^3 at times, t = 1 hr, and t = 2 hrs, respectively. These two figures show that vertical energy transport is more predominant for a number density of 100 particles/cm^3, than for 50 particles/cm^3, as the nucleation and condensation proceeds and the other parameters remain constant.

A comparison of visibility is also made for the case of different nuclei number densities. Figures 5 and 6 illustrate the visibility profiles for a nuclei number density of 50 particles/cm^3 at times, t = 1 hr, and t = 2 hrs, respectively. Figures 7 and 8 show similar visibility profiles for a nuclei number density of 100 particles/cm^3 at times, t = 1 hr, and t = 2 hrs, respectively. Comparison of Figures 5 and 7, and Figures 6 and 8, for one and two hours, respectively, after the cooling started, show

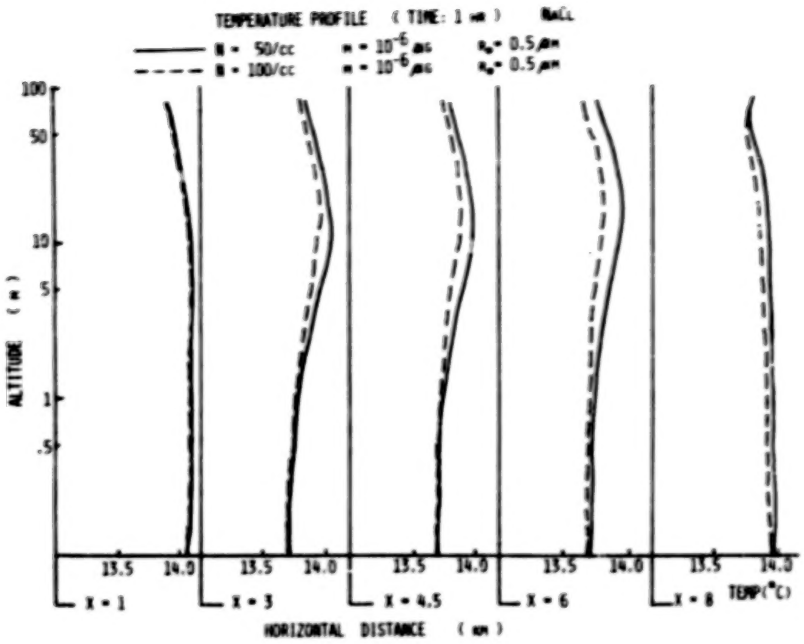

Figure 3. Comparison of temperature profiles of condensation nuclei, NaCl, between numbers of nuclei, 50 and 100 particles/cm^3, with constant mass of nucleus 10^{-6} μg, and radius of nucleus 0.5 μm, at time t = 1 hr.

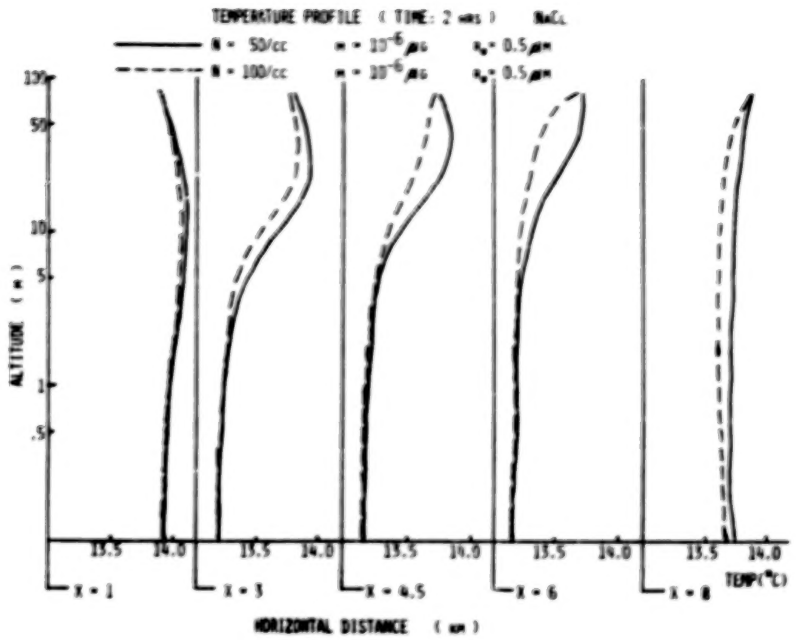

Figure 4. Comparison of temperature profiles of condensation nuclei, NaCl, between numbers of nuclei, 50 and 100 particles/cm^3, with constant mass of nucleus 10^{-6} μg, and radius of nucleus 0.5 μm, at time t = 2 hrs.

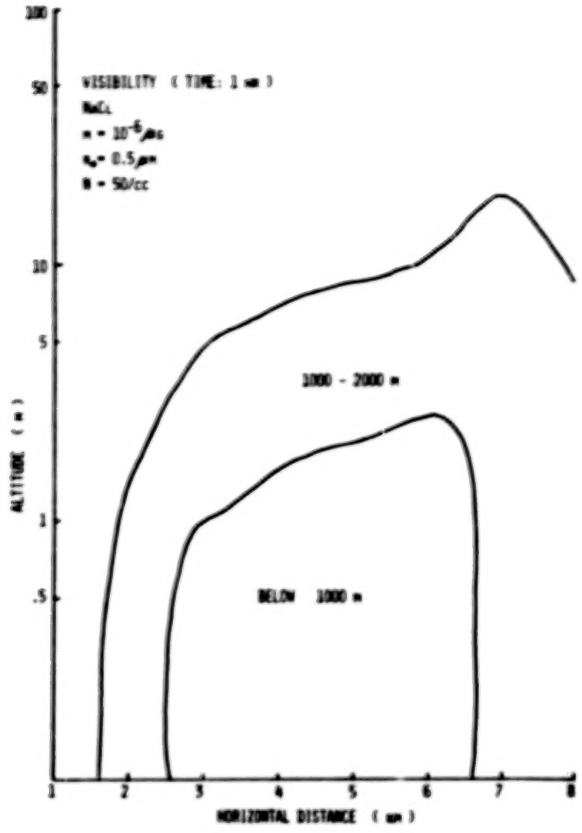

Figure 5. Visibility profile due to condensation nuclei, NaCl, with mass of nucleus 10^{-6} μg, radius of nucleus 0.5 μm, and number density 50 particles/cm^3, at time t = 1 hr.

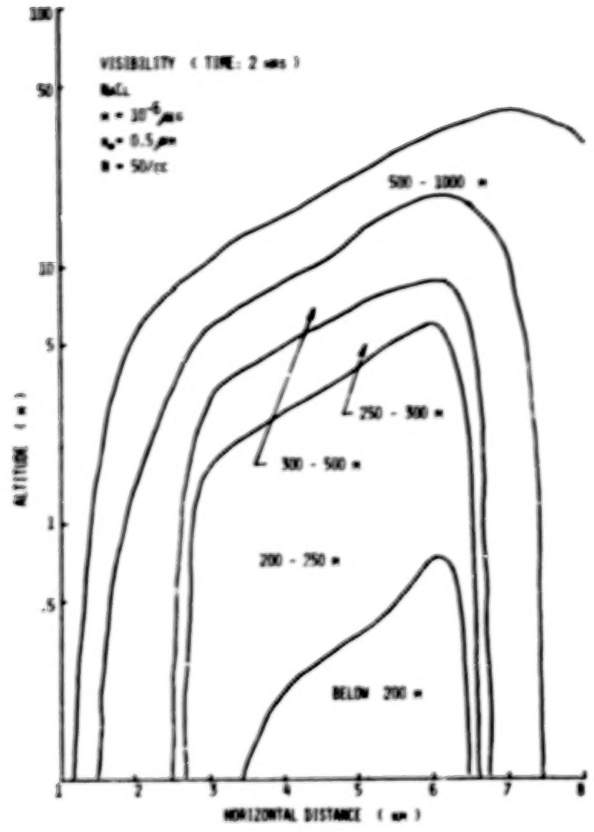

Figure 6. Visibility profile due to condensation nuclei, NaCl, with mass of nucleus 10^{-6} μg, radius of nucleus 0.5 μm, and number density 50 particles/cm^3, at time t = 2 hrs.

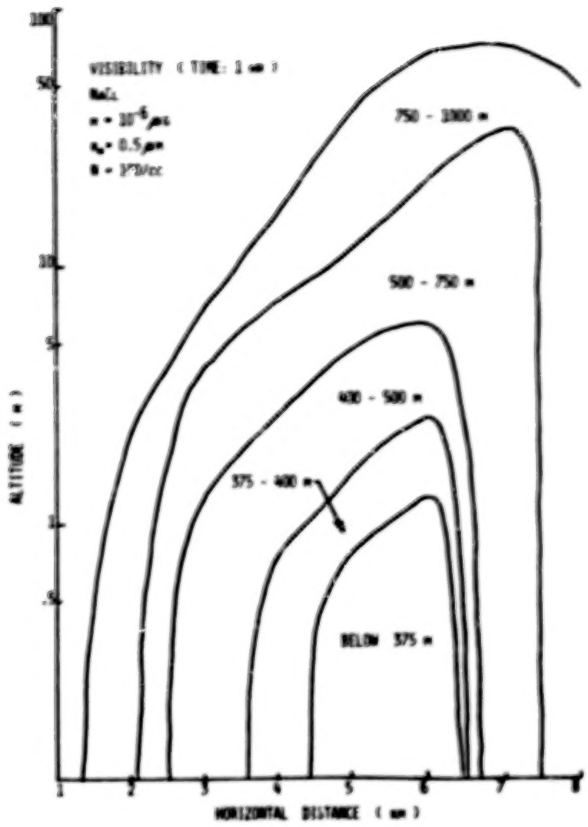

Figure 7. Visibility profile due to condensation nuclei, NaCl, with mass of nucleus 10^{-6} μg, radius of nucleus 0.5 μm, and number density 100 particles/cm^3, at time t = 1 hr.

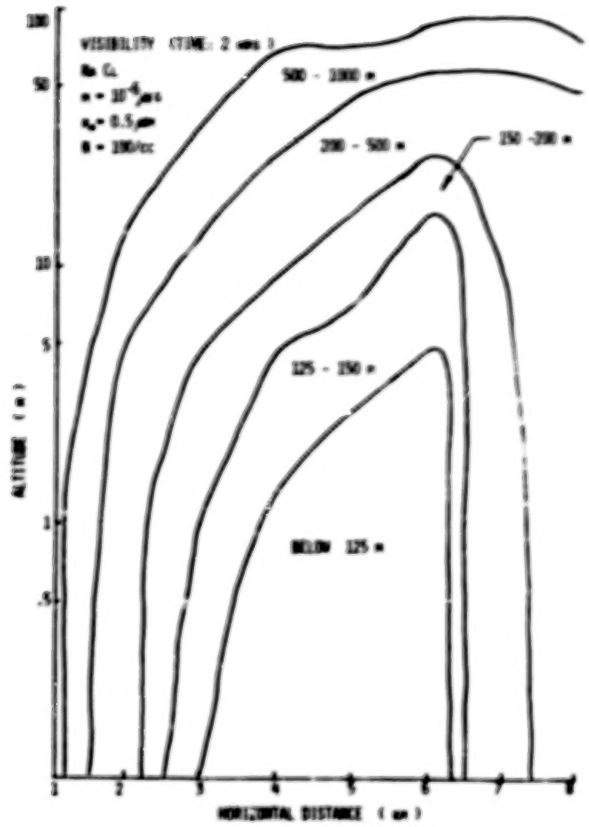

Figure 8. Visibility profile due to condensation nuclei, NaCl, with mass of nucleus 10^{-6} μg, radius of nucleus 0.5 μm, and number density 100 particles/cm^3, at time t = 2 hrs.

that a denser advection fog is formed for the cases with higher nuclei number densities.

Overall comparison of both temperature and visibility profiles indicate that higher numbers of sodium chloride nuclei per unit volume induce stronger vertical energy transfer and more favorable conditions for the formation of advection fog.

B. Mass of Nucleus as Variable

In this simulation, sodium chloride with nucleus size 1 μm radius, and numbers of nuclei, 100 particles/cm^3, is chosen for the computation. Figures 9 and 10 show the differences in the temperature profiles between masses of nucleus of 10^{-6} and 10^{-7} μg at times, t = 1 hr, and t = 2 hrs, respectively. These figures show that steeper temperature profiles are associated with the larger mass size. This also indicates that vertical energy transport is more enhanced for the larger mass size with the other parameters remaining constant.

Visibility changes resulting from the nucleation and condensation processes in the atmosphere were also computed. Figures 11 and 12 show the visibility profiles for a nucleus of mass 10^{-6} μg at times, t = 1 hr, and t = 2 hrs, respectively. Figures 13 and 14 show similar visibility profiles for a nucleus of mass 10^{-7} μg at times, t = 1 hr, and t = 2 hrs, respectively, after the initiation of cooling shows that lower visibility resulted for the case with the larger mass.

It can be concluded from this study that nuclei with heavier masses produce stronger vertical energy transport and also more favorable conditions for the formation of advection fog than nuclei of lighter masses.

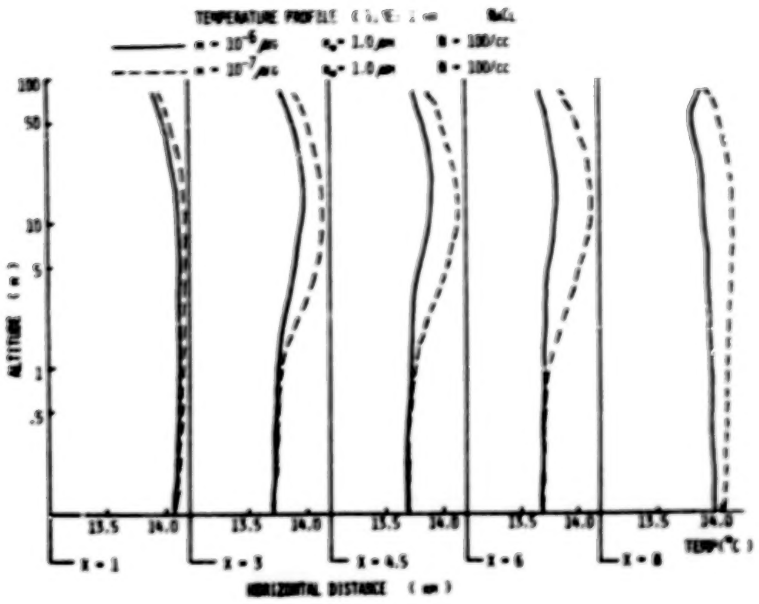

Figure 9. Comparison of temperature profiles of condensation nuclei, NaCl, between masses of nuclei, 10^{-6} and 10^{-7} μg, with constant radius of nucleus 1 μm, and number density 100 particles/cm^3, at time t = 1 hr.

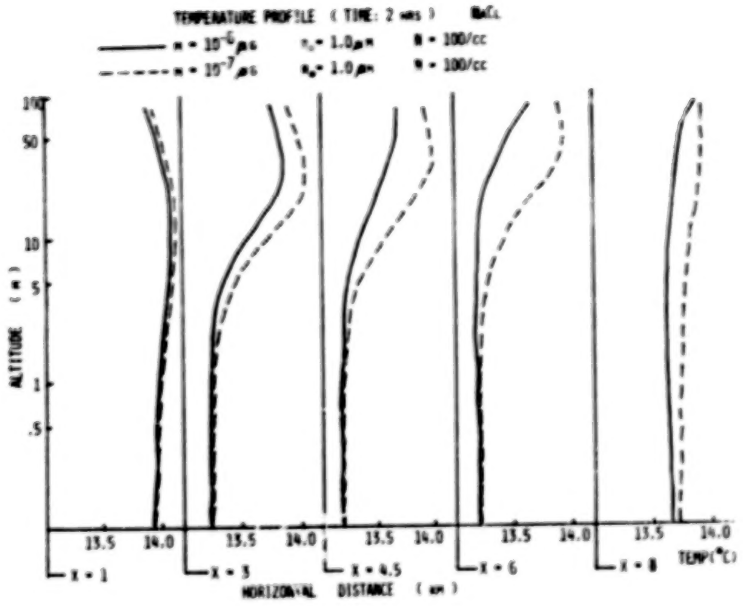

Figure 10. Comparison of temperature profiles of condensation nuclei, NaCl, between masses of nuclei, 10^{-6} and 10^{-7} μg, with constant radius of nucleus 1 μm, and number density 100 particles/cm^3, at time t = 2 hrs.

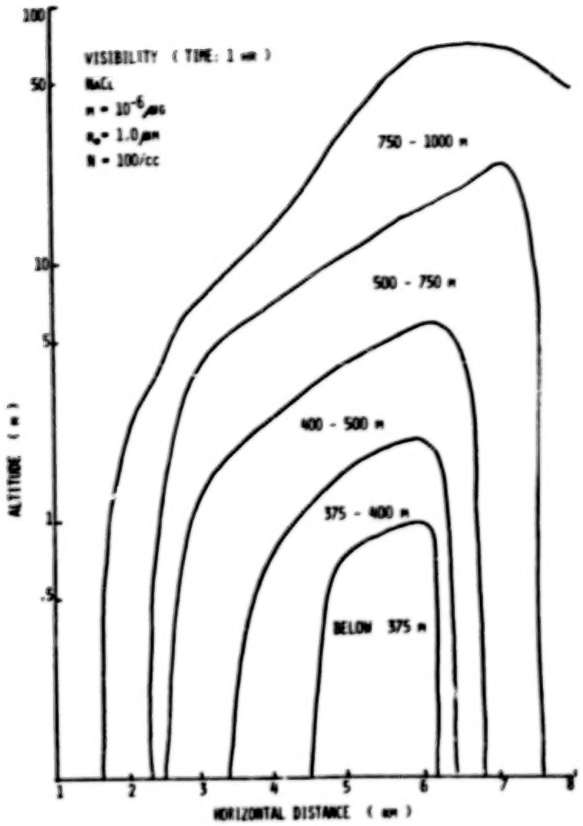

Figure 11. Visibility profile due to condensation nuclei, NaCl, with mass of nucleus 10^{-6} μg, radius of nucleus 1 μm, and number density 100 particles/cm^3, at time t = 1 hr.

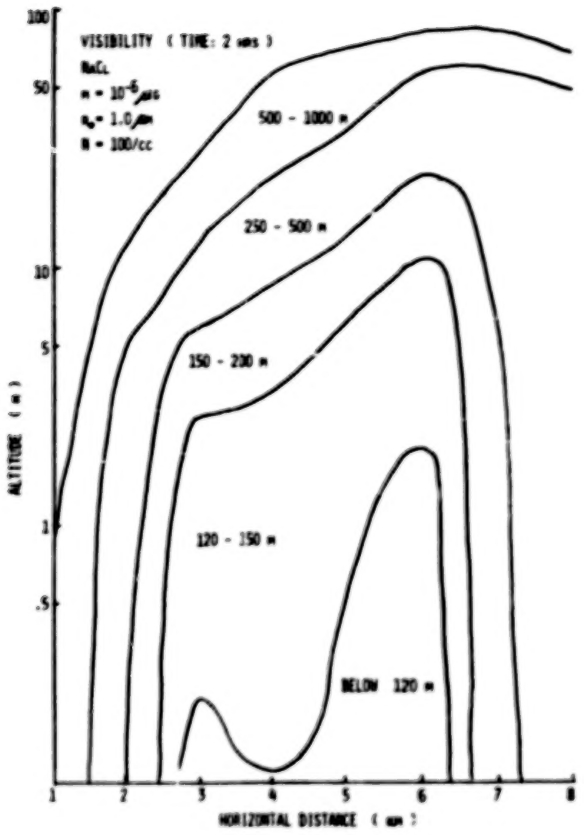

Figure 12. Visibility profile due to condensation nuclei, NaCl, with mass of nucleus 10^{-6} μg, radius of nucleus 1 μm, and number density 100 particles/cm^3, at time t = 2 hrs.

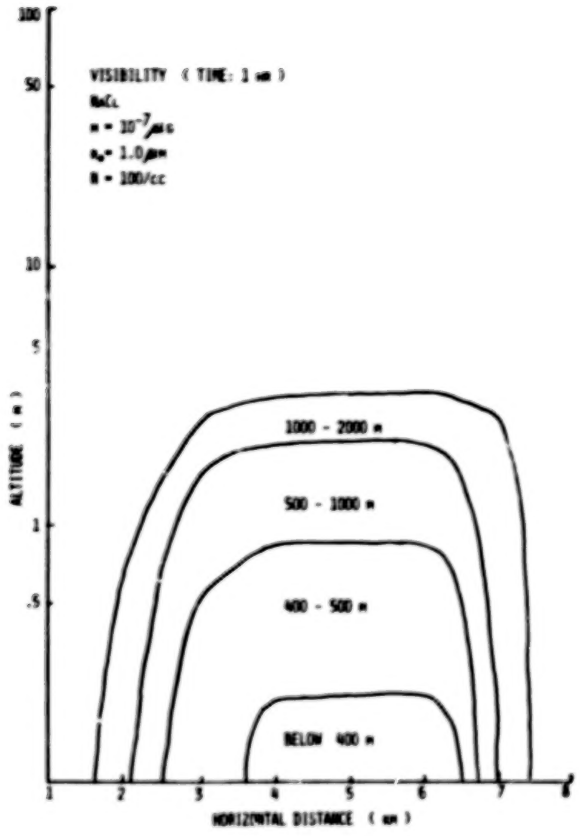

Figure 13. Visibility profile due to condensation nuclei, NaCl, with mass of nucleus 10^{-7} μg, radius of nucleus 1 μm, and number density 100 particles/cm^3, at time t = 1 hr.

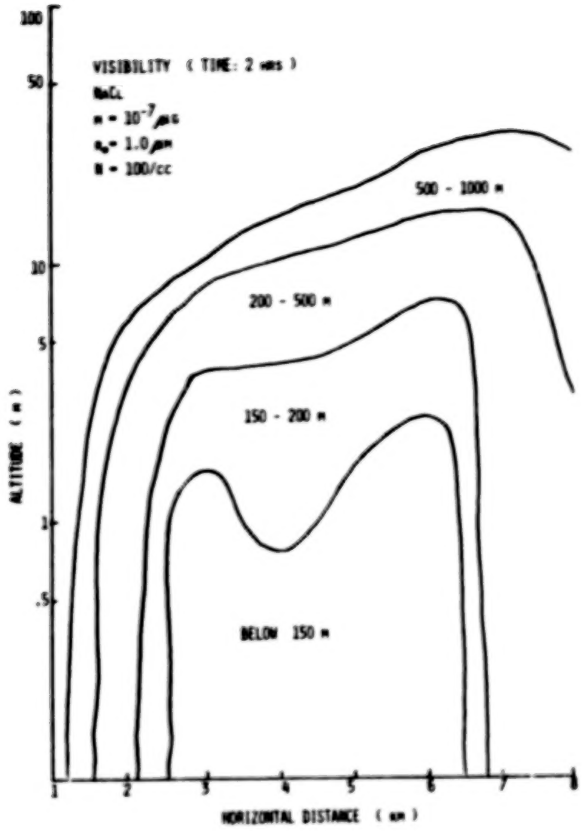

Figure 14. Visibility profile due to condensation nuclei, NaCl, with mass of nucleus 10^{-7} μg, radius of nucleus 1 μm, and number density 100 particles/cm^3, at time t = 2 hrs.

C. Radius of Nucleus as Variable

Effects of differences in radii of nuclei are studied using a constant background of sodium chloride with a nuclei number density of 100 particles/cm^3. Nuclei with radii of 0.5 and 1 μm and masses of 5.56×10^{-7} and 4.45×10^{-6} μg, respectively, are used. Figures 15 and 16 compare the temperature profiles for nuclei with radii of 0.5 and 1 μm at times, t = 1 hr, and t = 2 hrs, respectively. The vertical energy transport is more dominant for the nucleus with the radius of 1 μm than for the one with the 0.5 μm radius.

Comparison of visibility due to the nucleation and condensation for different size nuclei was also accomplished. Figures 17 and 18 show the visibility profiles for the nuclei with a radius 0.5 μm at times, t = 1 hr, and t = 2 hrs, respectively, while Figures 19 and 20 illustrate similar visibility profiles for the nuclei with a radius of 1 μm. Comparison of Figures 17 and 19, and Figures 18 and 20, for one and two hrs, respectively, after the air started to cool off, show that advection fog formed from nuclei with a radius of 1 μm had a much lower visibility than that formed from a nuclei with a radius of 0.5 μm.

Simulation of the nucleation and condensation process using different size sodium chloride nuclei shows that the nuclei with larger radii cause (1) a more pronounced vertical energy transport, and (2) a lower visibility than the nuclei with smaller radii.

IV. - AEROSOL PARTICLES WITH HIGHER RATIO OF THE VAN'T HOFF FACTOR TO MOLECULAR WEIGHT THAN SODIUM CHLORIDE AND THE FORMATION OF ADVECTION FOG

In the early stages of growth of a hygroscopic nucleus, the dependence on the Van't Hoff factor is very important. The Van't Hoff

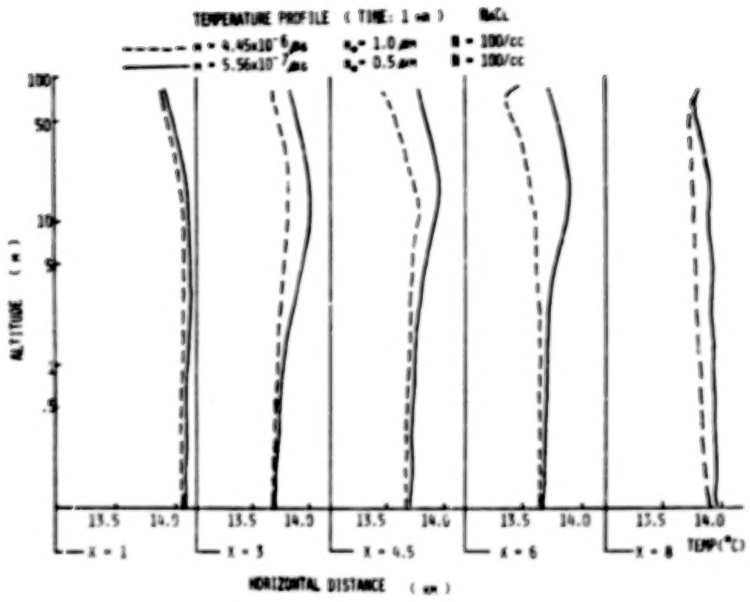

Figure 15. Comparison of temperature profiles of condensation nuclei, NaCl, between radii of nuclei, 1 and 0.5 μm, with corresponding masses of nuclei, 4.45×10^{-6} and 5.56×10^{-7} μg, respectively, and with constant number density 100 particles/cm^3, at time t = 1 hr.

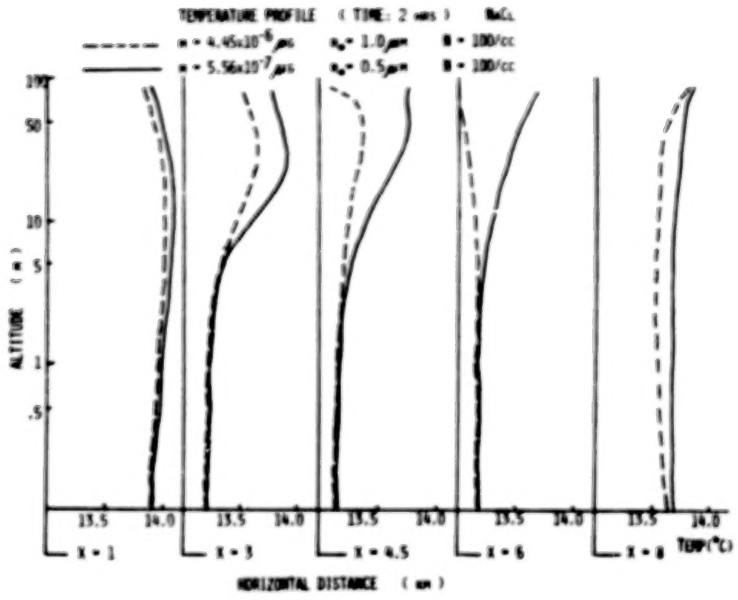

Figure 16. Comparison of temperature profiles of condensation nuclei, NaCl, between radii of nuclei, 1 and 0.5 μm, with corresponding masses of nuclei, 4.45×10^{-6} and 5.56×10^{-7} μg, respectively, and with constant number density 100 particles/cm^3, at time t = 2 hrs.

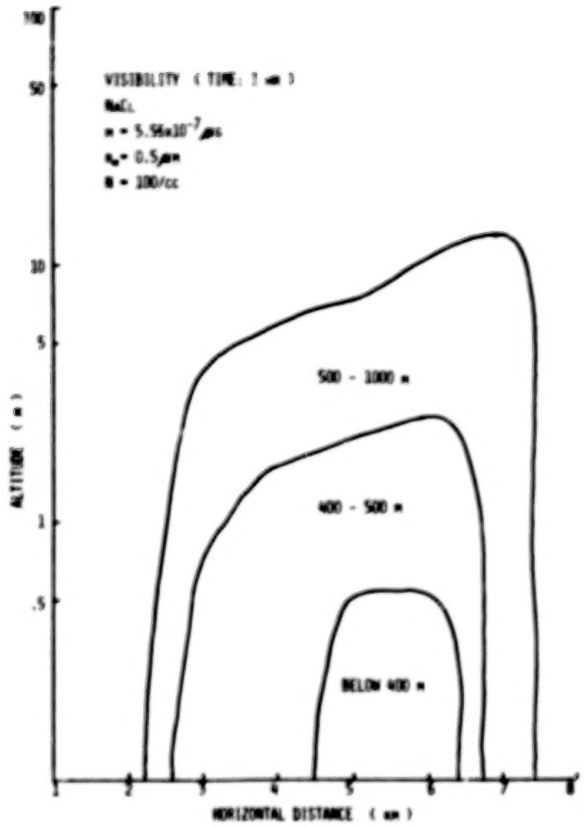

Figure 17. Visibility profile due to condensation nuclei, NaCl, with mass of nucleus 5.56×10^{-7} μg, radius of nucleus 0.5 μm, and number density 100 particles/cm^3, at time t = 1 hr.

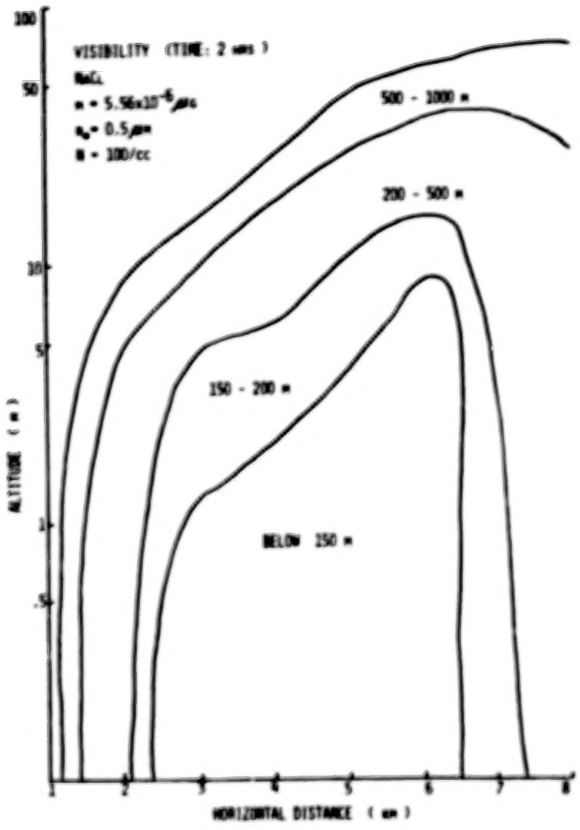

Figure 18. Visibility profile due to condensation nuclei, NaCl, with mass of nucleus 5.56×10^{-7} μg, radius of nucleus 0.5 μm, and number density 100 particles/cm^3, at time t = 2 hrs.

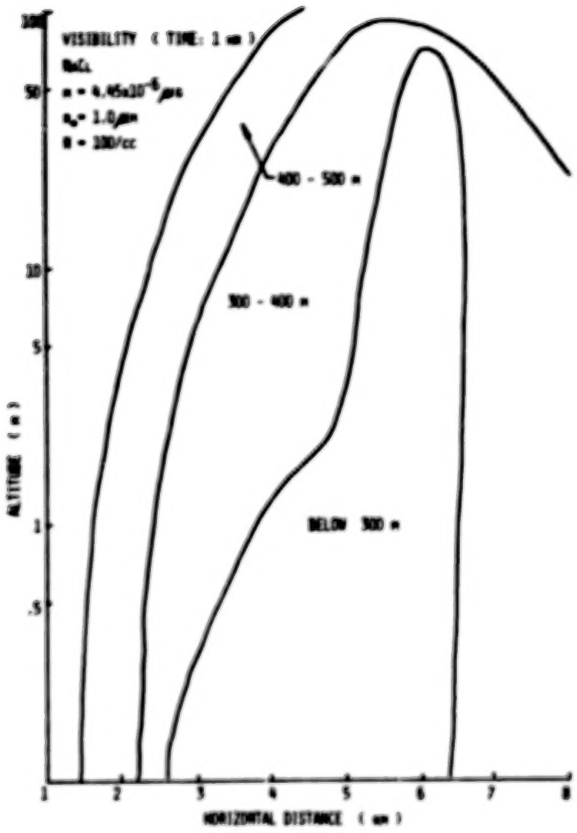

Figure 19. Visibility profile due to condensation nuclei, NaCl, with mass of nucleus 4.45×10^{-6} μg, radius of nucleus 1 μm, and number density 100 particles/cm^3, at time t = 1 hr.

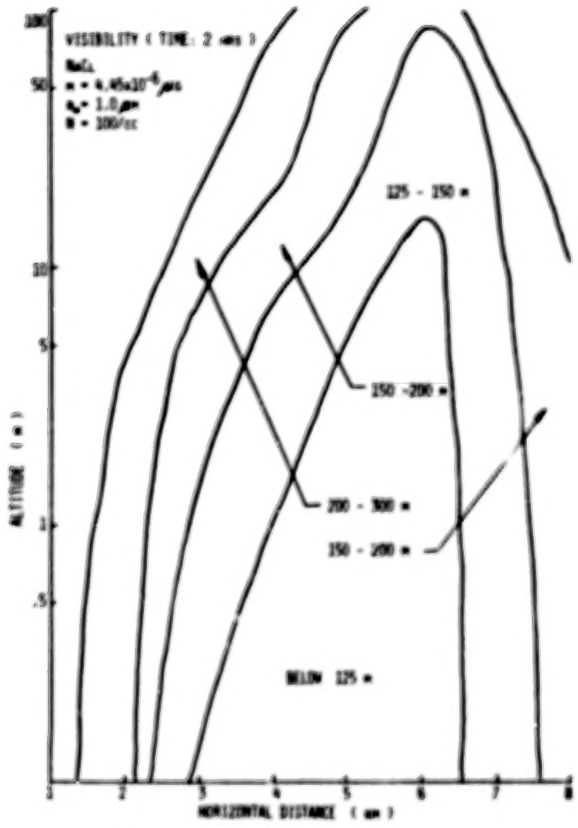

Figure 20. Visibility profile due to condensation nuclei, NaCl, with mass of nucleus 4.45×10^{-6} μg, radius of nucleus 1 μm, and number density 100 particles/cm^3, at time t = 2 hrs.

factor depends on the chemical nature and the degree of dissociation (i.e., on the concentration) of the solute. The ratio of the Van't Hoff factor, i., to the molecular weight of the hygroscopic nucleus, M, can be used as a measurement of nucleation and condensation for various species of hygroscopic chemicals. Table 1 shows i/M values of some hygroscopic chemicals and the values compared with that of sodium chloride. In this section, computed values of the vertical energy transport and visibility for hygroscopic chemicals of higher value i/M ratio than soidum chloriue are compared to the values for sodium chloride. Similar computations for hygroscopic chemicals with lower va ues of the i/M ratio are compared with that of sodium chloride in the next section.

Lithium chloride has an i/M ratio of 0.0482, and sodium chloride has an i/M ratio of 0.03257. The ratio of $(i/M)_{LiCl}$ to $(i/M)_{NaCl}$ which is 1.502, was chosen as an example in this study (Low, 1969). All the background conditions and geometries are similar to Section III. The nucleation and condensation processes using LiCl nuclei were compared to those using NaCl nuclei. The items compared are the same as A and B in Section III.

A. Case with Concentration of 50 $\mu g/m^3$ and Size of Nuclei of 0.5 μm Radius

In this case LiCl and NaCl with the same concentration, 50 $\mu g/m^3$ (mass of nucleus, 10^{-6} μg, and number of nuclei, 50 particles/cm^3) and nuclei size, 0.5 μm radius were used to study changes in vertical energy transport and visibility as the nucleation and condensation processes progressed. Figures 21 and 22 compare the temperature profiles for the LiCl nuclei and NaCl nuclei at times, t = 1 hr, and t = 2 hrs, respectively. These two figures show that the vertical energy transport was stronger for the LiCl nuclei than for the NaCl nuclei.

Table I. Comparison of Ratio of Van't Hoff Factor to Molecular Weight for Some Typical Hygroscopic Materials

Hygroscopic Materials	*Van't Hoff Factor, i	Molecular Weight, M	Ratio i/M	Comparison of (i/M) With NaCl
$Ca(NO_3)_2$	2.638	164.1	0.01608	0.4937
KCl	1.823	74.56	0.02445	0.7507
$CaCl_2$	3.228	111	0.02908	0.8928
NaCl	1.904	58.45	0.03257	1
LiCl	2.074	42.4	0.04892	1.5020

*Van't Hoff factor is measured at 25°C, 1 atm, and 1 molality.

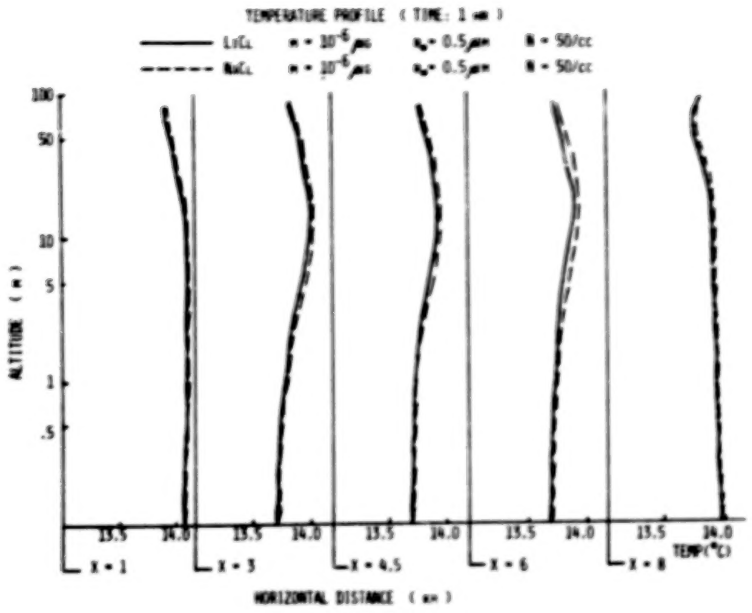

Figure 21. Comparison of temperature profiles between condensation nuclei, LiCl and NaCl, with the same mass of nucleus 10^{-6} μg, radius of nucleus 0.5 μm, and number density 50 particles/ cm^3, at time t = 1 hr.

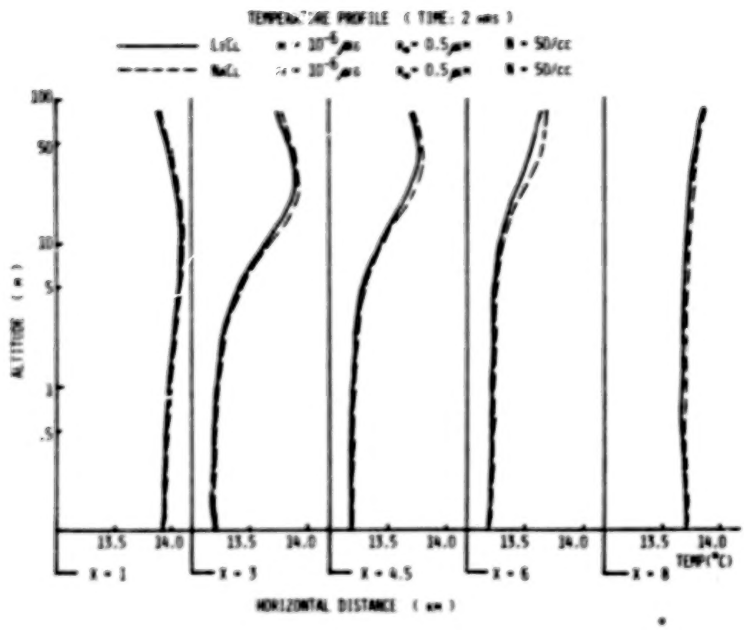

Figure 22. Comparison of temperature profiles between condensation nuclei, LiCl and NaCl, with the same mass of nucleus 10^{-6} μg, radius of nucleus 0.5 μm, and number density 50 particles/ cm^3, at time t = 2 hrs.

Figures 23 and 24 show the visibility profiles for the LiCl nuclei at times, t = 1 hr, and t = 2 hrs, respectively. Comparison of Figures 23 and 5, and Figures 24 and 6, shows that denser advection fog is formed by the LiCl nuclei than by the NaCl nuclei.

B. Case with Concentration of 100 $\mu g/m^3$ and Size of Nuclei of 1 μm Radius

In this case LiCl and NaCl with the same concentration, 100 $\mu g/m^3$ (the mass of the nucleus, 10^{-6} μg, and number of nuclei, 100 particles/cm^3) and nuclei size, 1 μm radius, were used. Figures 25 and 26 compare the temperature profiles for LiCl and NaCl nuclei cases at times, t = 1 hr, and t = 2 hrs, respectively. These figures also show that the vertical energy transport was more enhanced for the LiCl nuclei than for the NaCl nuclei.

Visibility resulting from the nucleation and condensation on LiCl nuclei for this particular case is shown in Figures 27 and 28 for times, t = 1 hr, and t = 2 hrs, respectively. Comparisons of Figures 27 and 11, and Figures 28 and 12, show that a lower visibility advection fog was formed from the LiCl nuclei than from the NaCl nuclei.

It can be concluded from the present study that aerosol particles with higher ratios of i/M than sodium chloride cause more pronounced vertical energy transport and also denser fogs.

V. - AEROSOL PARTICLES WITH LOWER RATIO OF VAN'T HOFF FACTOR TO MOLECULAR WEIGHT THAN SODIUM CHLORIDE AND THE FORMATION OF ADVECTION FOG

Two hygroscopic chemicals with lower ratios of (i/M) than that of sodium chloride are chosen in this study. The chemicals chosen were calcium nitrate, $(i/M)_{Ca(NO_3)_2} = 0.01608$ and calcium chloride, $(i/M)_{CaCl_2} = 0.02908$. The ratio of $(i/M)_{Ca(NO_3)_2}$ to $(i/M)_{NaCl}$ is 0.4937; and ratio

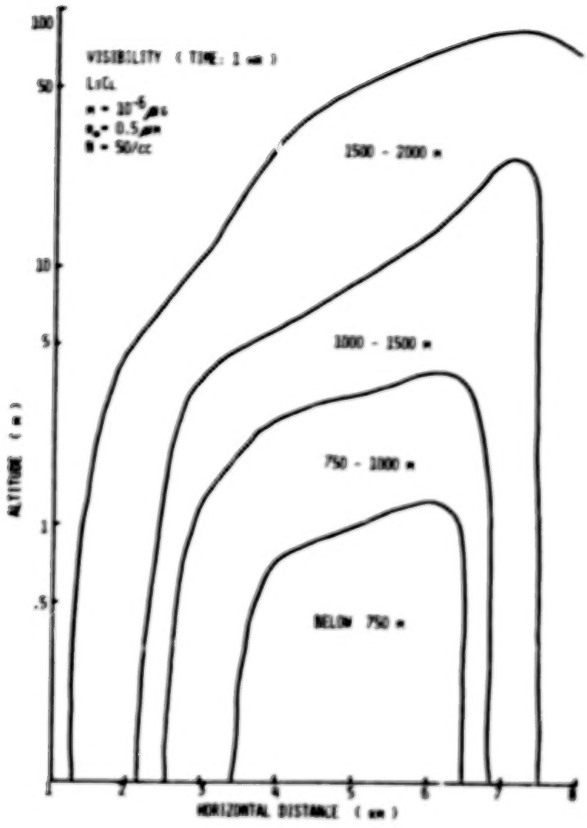

Figure 23. Visibility profile due to condensation nuclei, LiCl, with mass of nucleus 10^{-6} μg, radius of nucleus 0.5 μm, and number density 50 particles/cm^3, at time t = 1 hr.

Figure 24. Visibility profile due to condensation nuclei, LiCl, with mass of nucleus 10^{-6} μg, radius of nucleus 0.5 μm, and number density 50 particles/cm^3, at time t = 2 hrs.

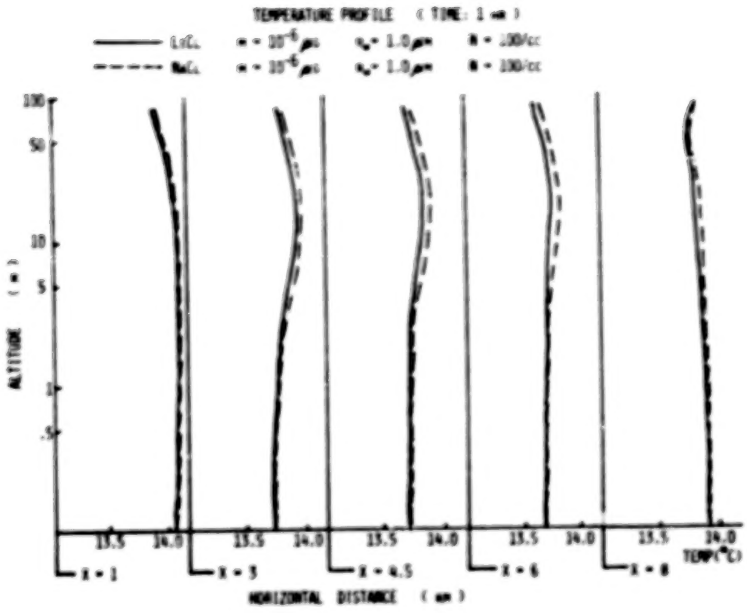

Figure 25. Comparison of temperature profiles between condensation nuclei, LiCl and NaCl, with the same mass of nucleus 10^{-6} μg, radius of nucleus 1 μm, and number density 100 particles/ cm^3, at time t = 1 hr.

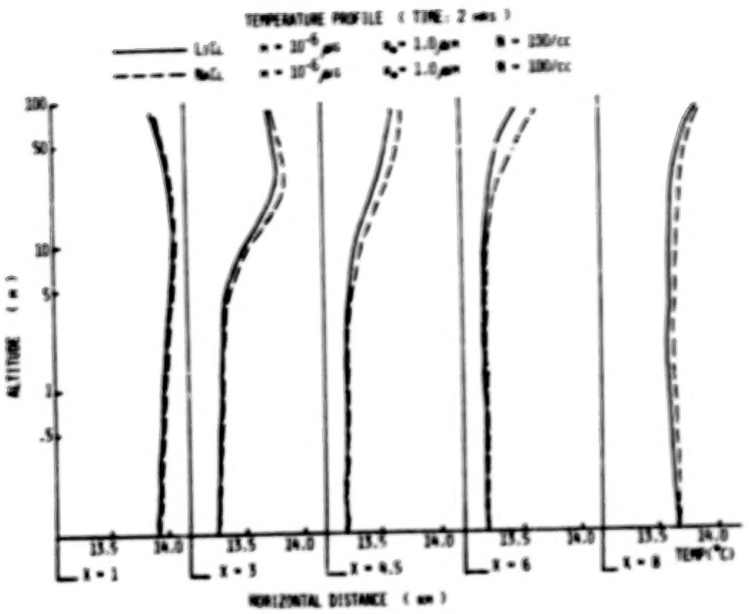

Figure 26. Comparison of temperature profiles between condensation nuclei, LiCl and NaCl, with the same mass of nucleus 10^{-6} μg, radius of nucleus 1 μm, and number density 100 particles/ cm^3, at time t = 2 hrs.

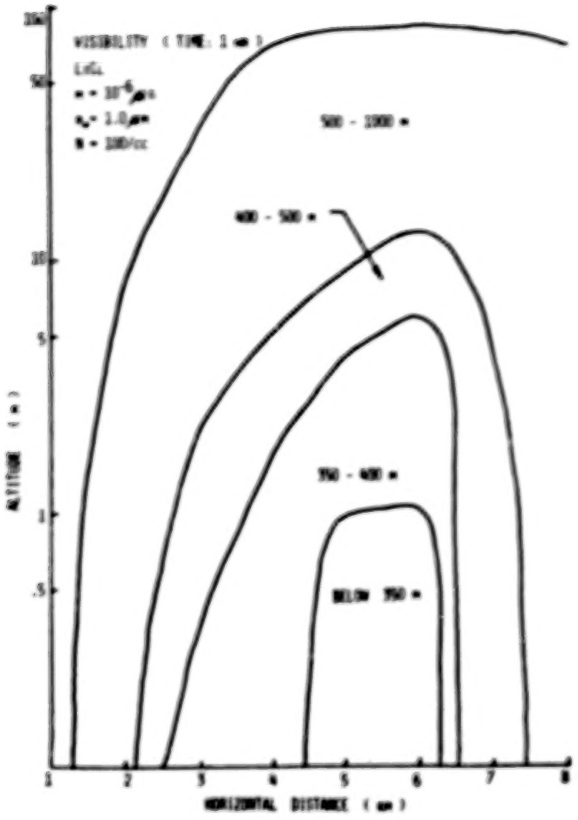

Figure 27. Visibility profile due to condensation nuclei, LiCl, with mass of nucleus 10^{-6} μg, radius of nucleus 1 μm, and number density 100 particles/cm^3, at time t = 1 hr.

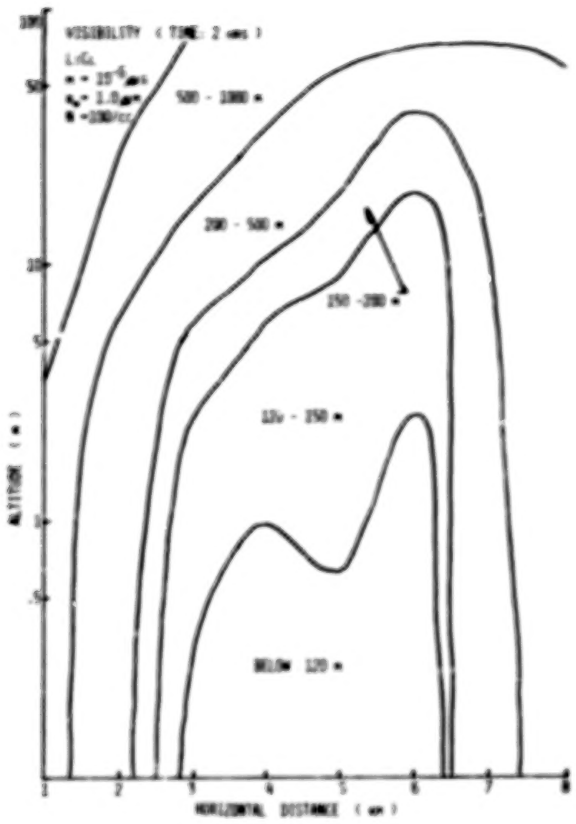

Figure 28. Visibility profile due to condensation nuclei, LiCl, with mass of nucleus 10^{-6} μg, radius of nucleus 1 μm, and number density 100 particles/cm^3, at time t = 2 hrs.

of $(i/M)_{CaCl_2}$ to $(i/M)_{NaCl}$ is 0.8928. All the background conditions and geometries used are similar to Section III. The items of comparison are also from A and B in Section III.

A. Case with Concentration of 100 $\mu g/m^3$ and Size of Nuclei of 0.5 μm Radius

In this case $Ca(NO_3)_2$ and NaCl with the same concentration, 100 $\mu g/m^3$ (mass of nucleus, 10^{-6} μg, and number of nuclei, 100 particles/cm^3) and nuclei size, 0.5 μm radius were used. Figures 29 and 30 compare the temperature profiles for the $Ca(NO_3)_2$ nuclei and NaCl nuclei at times, t = 1 hr, and t = 2 hrs, respectively. These two figures indicate that the vertical energy transport was more enhanced for the NaCl nuclei than for the $Ca(NO_3)_2$ nuclei.

Visibility resulting from the nucleation and condensation caused by $Ca(NO_3)_2$ nuclei is shown in Figures 31 and 32 at times, t = 1 hr, and t = 2 hrs, respectively. Comparisons of Figures 31 and 7, and Figures 32 and 8, show that lower visibility advection fog was formed from the NaCl nuclei than from the $Ca(NO_3)_2$ nuclei.

Visibility of advection fog caused by $CaCl_2$ nuclei under the same background conditions, and the same concentration and nuclei size was also numerically simulated. Figures 33 and 34 show the visibility of the advection fog due to $CaCl_2$ at times, t = 1 hr, and t = 2 hrs, respectively. Comparisons of Figures 33, 31 and 7 for the one hour case; and Figures 34, 32 and 8 for the two hour case, indicate that $V_{NaCl} < V_{CaCl_2} < V_{Ca(NO_3)_2}$, where V denotes visibility, which correlates with the ratios $(i/M)_{NaCl} > (i/M)_{CaCl_2} > (i/M)_{Ca(NO_3)_2}$ for a concentration of 100 $\mu g/m^3$ and a nuclei radius of 0.5 μm. Similar results are also obtained for the vertical energy transfer; in this case, the higher the value of (i/M), the more

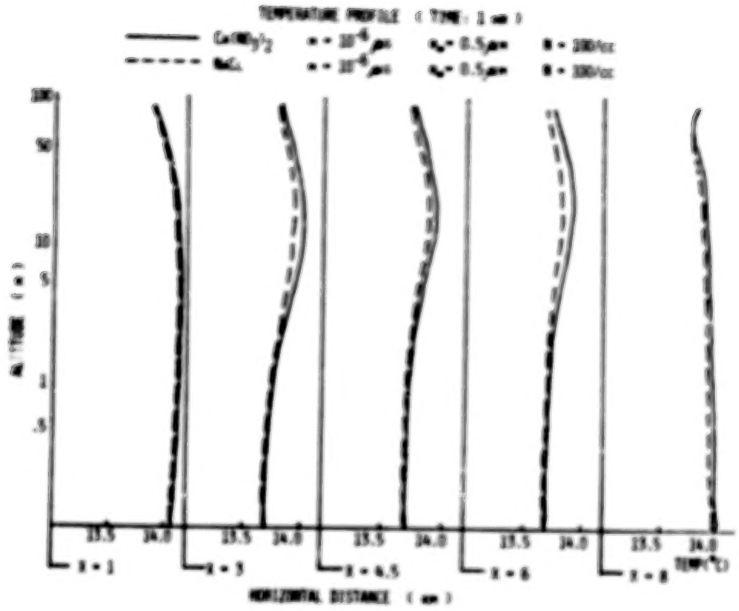

Figure 29. Comparison of temperature profiles between condensation nuclei, $Ca(NO_3)_2$ and NaCl, with the same mass of nucleus 10^{-6} μg, radius of nucleus 0.5 μm, and number density 100 particles/cm^3, at time t = 1 hr.

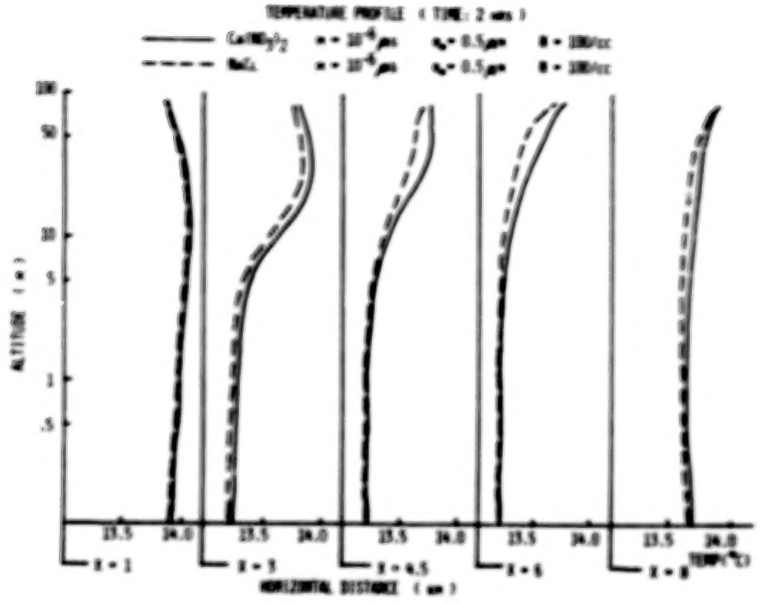

Figure 30. Comparison of temperature profiles between condensation nuclei, $Ca(NO_3)_2$ and NaCl, with the same mass of nucleus 10^{-6} μg, radius of nucleus 0.5 μm, and number density 100 particles/cm^3, at time t = 2 hrs.

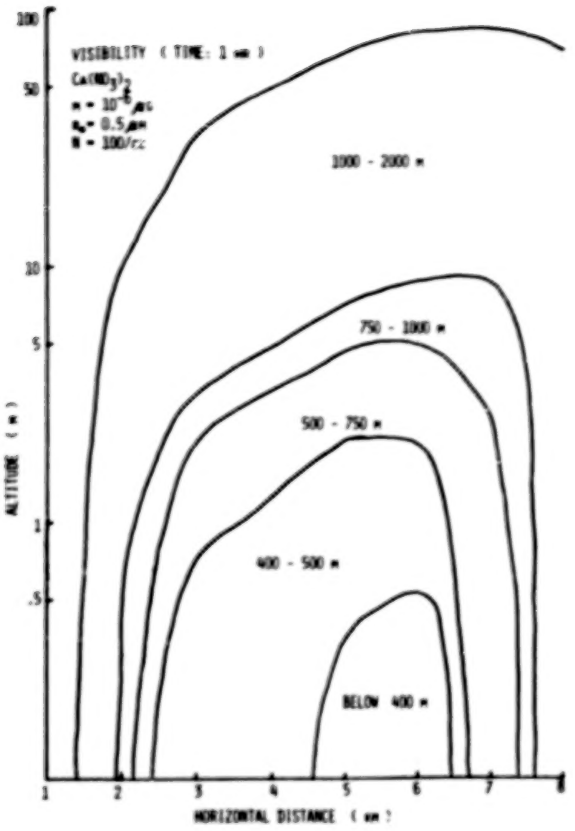

Figure 31. Visibility profile due to condensation nuclei, $Ca(NO_3)_2$, with mass of nucleus 10^{-6} μg, radius of nucleus 0.5 μm, and number density 100 particles/cm^3, at time t = 1 hr.

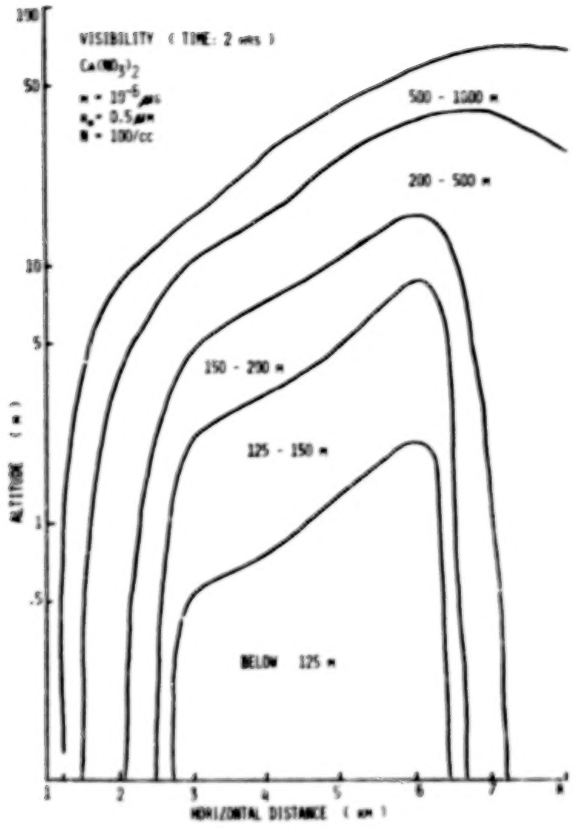

Figure 32. Visibility profile due to condensation nuclei, $Ca(NO_3)_2$, with mass of nucleus 10^{-6} μg, radius of nucleus 0.5 μm, and number density 100 particles/cm^3, at time t = 2 hrs.

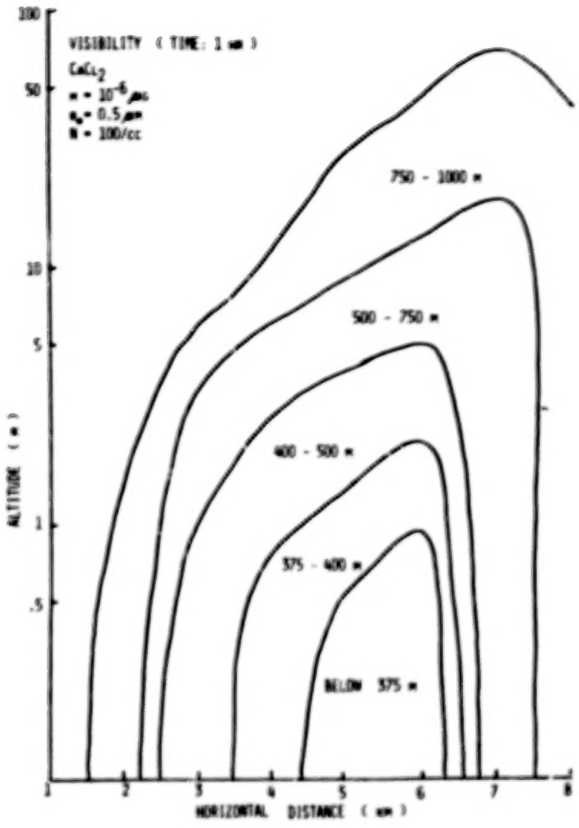

Figure 33. Visibility profile due to condensation nuclei, $CaCl_2$, with mass of nucleus 10^{-6} μg, radius of nucleus 0.5 μm, and number density 100 particles/cm^3, at time t = 1 hr.

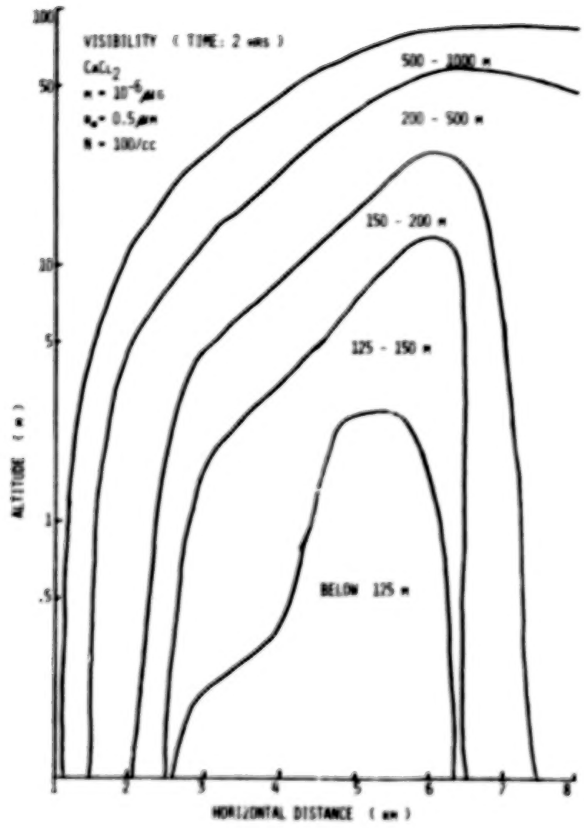

Figure 34. Visibility profile due to condensation nuclei, $CaCl_2$, with mass of nucleus 10^{-6} μg, radius of nucleus 0.5 μm, and number density 100 particles/cm^3, at time t = 2 hrs.

pronounced the vertical energy transfer.

B. Case with Concentration of 100 $\mu g/m^3$ and the Size of Nuclei of 1 μm Radius

In this case $CaCl_2$ and NaCl with the same concentration, 100 $\mu g/m^3$ (mass of nucleus, 10^{-6} μg, and number of nuclei, 100 particles/cm^3) and nuclei size, 1 μm radius were used. Figures 35 and 36 compare the temperature profiles for $CaCl_2$ and NaCl at times, t = 1 hr, and t = 2 hrs, respectively. The visibility profiles of $CaCl_2$ are shown in Figures 37 and 38 at times, t = 1 hr, and t = 2 hrs, respectively. Comparisons of the temperature profiles and the visibility profiles of Figures 37 and 11, and Figures 38 and 12 all show the same conclusions as Section IV-A; the higher the value of (i/M), the stronger the vertical energy transfer and the denser the fog formed.

VI. - CONCLUSIONS AND DISCUSSIONS

The present study demonstrates the capability of numerically simulating the formation of warm advection fog. By using observed initial values of the wind profile, the temperature profile, the humidity, the possible cooling rate, or the temperature change expected, and the aerosol particle characteristics, including chemical composition, mass of nuclei, particle size and the number of nuclei per unit volume, we are able to produce fogs. The results of the simulations are in reasonably good agreement with field observations from the California coast made by Mack et al. (1973; 1974; and 1975), although a detailed comparison is not possible at this time because of the limited number of time dependent measurements of dynamic conditions and aerosol data in the vertical coordinates.

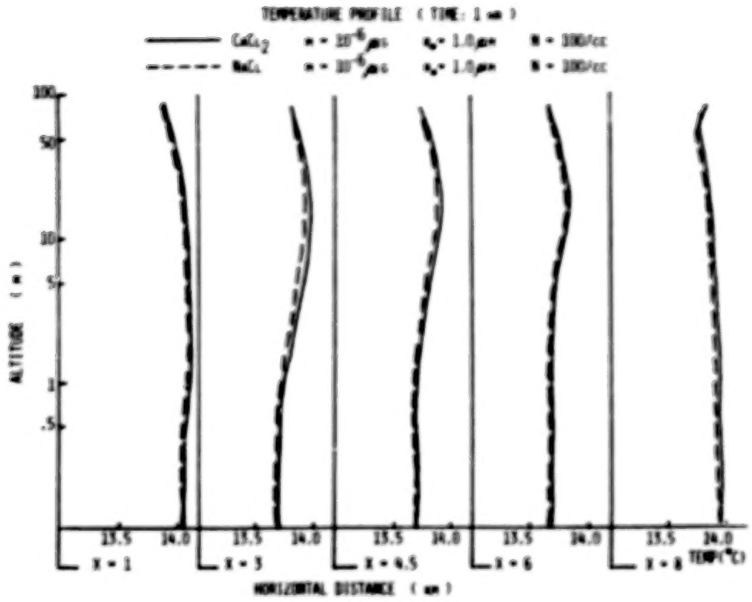

Figure 35. Comparison of temperature profiles between condensation nuclei, $CaCl_2$ and NaCl, with the same mass of nucleus 10^{-6} μg, radius of nucleus 1μm, and number density 100 particles/cm^3, at time t = 1 hr.

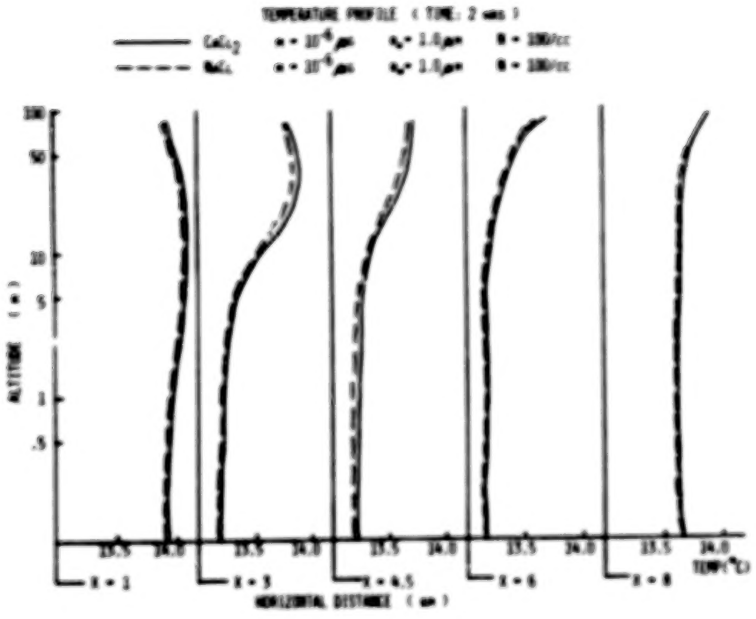

Figure 36. Comparison of temperature profiles between condensation nuclei, $CaCl_2$ and NaCl, with the same mass of nucleus 10^{-6} μg, radius of nuclius 1 μm, and number density 100 particles/cm^3, at time t = 2 hrs.

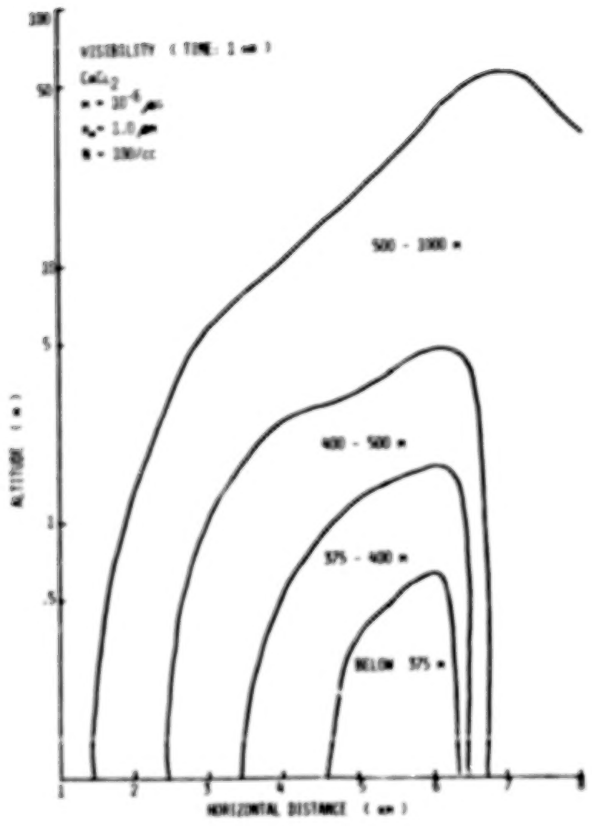

Figure 37. Visibility profile due to condensation nuclei, $CaCl_2$, with mass of nucleus 10^{-6} μg, radius of nucleus 1 μm, and number density 100 particles/cm^3 at time t = 1 hr.

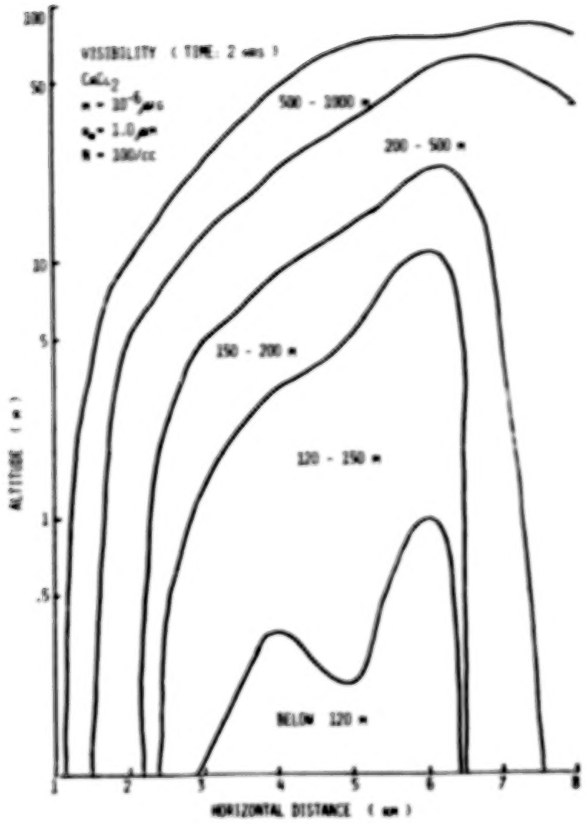

Figure 38. Visibility profile due to condensation nuclei, $CaCl_2$, with mass of nucleus 10^{-6} μg, radius of nucleus 1 μm, and number density 100 particles/cm^3 at time t = 2 hrs.

This study of the correlation of the characteristics of aerosol particles and the formation of advection fog provides the following conclusions:

(1) Hygroscopic chemicals with a higher ratio of the Van't Hoff factor to molecular weight produce a more enhanced rate of vertical energy transfer and more favorable conditions for denser advection fog than chemicals with lower values of the ratio.

(2) A higher number density of aerosol nuclei increases the rate of the vertical energy transfer and produces advection fog with lower visibility during the nucleation and condensation processes than a lower nuclei number density.

(3) Heavier mass nuclei aerosol particles favor the formation of advection fog with a lower visibility and a higher rate of vertical energy transfer than do lighter mass nuclei during the nucleation processes.

(4) CCN with larger radii cause stronger vertical energy transfer and a denser advection fog during the nucleation and condensation period than CCN with smaller radii.

Baker, E. H. (1977). - A maritime boundary layer model for the prediction of fog. Bound-Layer Meteor., 11, pp. 267-294.

Eadie, W. J., Rogers, C. W., Katz, U., and Kocmond, W. C. (1975). - Project Fog Drops V. Part I: A numerical model of advection fog. Report NASA CR-2633, Calspan Corp., 54 p.

Fitzgerald, J. W. (1978). - A numerical model of the formation of droplet spectra in advection fogs at sea and its applicability to fogs off Nova Scotia. J. Atmos. Sci., 35, pp. 1522-1535.

Fletcher, N. H. (1966). - The Physics of Rain Clouds, Cambridge Univ. Press, Cambridge, England, 390p.

Hung, R. J., and Huckle, J. R. (1977). - Accuracy of initial dew point temperature and the growth of droplet in expansion chamber under low gravity environment. J. Rech. Atmos., 11, pp. 165-178.

Hung, R. J., Liaw, G. S., and Vaughan, O. H. (1978). - Numerical simulation of warm fog and its application to warm fog prediction and modification. Proc. Atmospheric Environment of Aerospace Systems and Applied Meteorology, Am. Meteor. Soc., Boston, Mass., pp. 169-173.

Hung, R. J., and Vaughan, O. H. (1977). - Numerical simulation of life cycles of advection warm fog. AIAA Paper No. 77-130, 9p.

Isono, K. (1957). - On sea-salt nuclei in the atmosphere. Geofis. Pura Appl. 36, pp. 156-165.

Low, R. D. H. (1969). - A generalized equation for solution effect in droplet growth. J. Atmos. Sci., 26, pp. 608-611.

Mack, E. J., Pilie, R. J. and Kockmond, W. C. (1973). - An Investigation of the Microphysical and Micrometeorological Properties of Sea Fog, Calspan Corp., New York, 33p.

Mack, E. J., Katz, U., Rogers, C. W. and Pilie, R. J. (1974). - The Microstructure of California Coastal Stratus and Fog at Sea,

Calspan Corp., New York, 67p.

Mack, E. J., Pilie, R. J. and Katz, U. (1975). - Marine Fog Studies off the California Coast, Calspan Corp., New York, 69p.

Mason, B. J. (1971). - The Physics of Clouds, 2nd Edition, Clarendon Press, Oxford, 671p.

Richtmeyer, R. D. (1957). - Difference Methods for Initial-Value Problems, Interscience Publ., New York, 238p.

Sax, R. I., Changnon, S. A., Grant, L. O., Hitschfeld, W. F., Hobbs, P. V., Kahan, A. M., and Simpson, J. (1975). - Weather modification: where are we now and where should we be going? An editorial overview. J. Appl. Meteor., 14, pp. 652-672.

Silverman, B. A., and Weinstein, A. I. (1974). - Fog, in Weather and Climate Modification, ed. by N. Hess, John Wiley, New York, pp. 355-384.

Weinstein, A. I., and Silverman, B. A. (1973). - A numerical analysis of some practical aspects of airborne area seeding for warm fog dispersal at airports. J. Appl. Meteor., 12, pp. 771-780.

1. REPORT NO.	2. GOVERNMENT ACCESSION NO.	3. RECIPIENT'S CATALOG NO.
NASA CR-3085		

4. TITLE AND SUBTITLE	5. REPORT DATE
Hygroscopic Chemicals and the Formation of Advection Warm Fog—A Numerical Simulation	December 1978
	6. PERFORMING ORGANIZATION CODE
7. AUTHOR(S)	8. PERFORMING ORGANIZATION REPORT #
R. J. Hung and G. S. Liaw	
9. PERFORMING ORGANIZATION NAME AND ADDRESS	10. WORK UNIT NO.
The University of Alabama in Huntsville Huntsville, Alabama	M-278
	11. CONTRACT OR GRANT NO.
	NAS8-31729
	13. TYPE OF REPORT & PERIOD COVERED
12. SPONSORING AGENCY NAME AND ADDRESS	Contractor
National Aeronautics and Space Administration Washington, D. C. 20546	14. SPONSORING AGENCY CODE

15. SUPPLEMENTARY NOTES

Prepared under technical monitorship of the Atmospheric Sciences Division, Space Sciences Laboratory, NASA Marshall Space Flight Center

16. ABSTRACT

The formation of advection fog is closely associated with the characteristics of the aerosol particles, including the chemical composition, mass of the nuclei, particle size, and concentration. Both macrophysical and microphysical processes are considered. In the macrophysical model, the evolution of wind components, water vapor content, liquid water content and potential temperature under the influences of vertical turbulent diffusion, turbulent momentum, and turbulent energy transfers are taken into account. In the microphysical model, the supersaturation effect is incorporated with the surface tension and hygroscopic material solution. The results show that the aerosol particles with the higher number density, larger size nuclei, the heavier mass of the nuclei, and the higher ratio of the Van't Hoff factor to the molecular weight favor the formation of the lower visibility advection fogs with stronger vertical energy transfer during the nucleation and condensation time period.

17. KEY WORDS	18. DISTRIBUTION STATEMENT
Aerosol Particles Hygroscopic Chemicals Fog Microphysics Advection Warm Fog Numerical Simulation	Category 47

19. SECURITY CLASSIF. (of this report)	20. SECURITY CLASSIF. (of this page)	21. NO. OF PAGES	22. PRICE
Unclassified	Unclassified	65	$5.25

MSFC

* For sale by the National Technical Information Service, Springfield, Virginia 22161

NASA-Langley, 1978

END

MAR 6 1979